Octopaminergic neurons have multiple targets in *Drosophila* larval mushroom body calyx and regulate behavioral odor discrimination

Authors

Alex D McLachlan,[1] J Y Hilary Wong,[1] Bo Angela Wan,[1] Cahir J O'Kane, Marcella Montagnese, Shuo Wei Zhang, Liria M Masuda-Nakagawa*

Department of Genetics, University of Cambridge, UK

[1] These authors contributed equally

*** Correspondence to LMM-N**

lm546@gen.cam.ac.uk

Department of Genetics

University of Cambridge

Downing Street

Cambridge, CB2 3EH

United Kingdom

Abstract

Behavior depends on discrimination of selective sensory representations. These are modified dynamically by changes in behavioral state, facilitating context-dependent selection of behavior. These are mediated by brain signals carried by noradrenergic input in mammals, or octopamine (OA) in insects. To understand the circuit mechanisms of this signaling, we characterized the function of two OA neurons, in the input region to the memory center, the mushroom body calyx, in larval *Drosophila*. Here they target multiple neurons, including olfactory projection neurons (PNs), the inhibitory neuron APL, a pair of extrinsic output neurons, but relatively few mushroom body intrinsic neurons, Kenyon cells. The OA receptor Oamb, a *Drosophila* α1-adrenergic receptor ortholog, localized to PN terminals, and optogenetic activation of OA neurons both potentiated PN activity, and compromised odor discrimination behavior. Our results suggest that OA neurons gate odor signals for sensory processing via extrinsic inputs at the input to the olfactory learning circuit.

Introduction

Behavioral choices depend on discrimination among "sensory objects", which are neural representations of multiple coincident sensory inputs, across a range of sensory modalities. For example, "odor objects" (Gottfried, 2009; Wilson and Sullivan, 2011; Gire et al., 2013) are represented in sparse ensembles of neurons, that are coincidence detectors of multiple parallel inputs from odor quality channels. This principle is used widely in animals, including in mushroom bodies (MBs), the insect center for associative memory (Masuda-Nakagawa et al. 2005; Honegger et al. 2011), and in the piriform cortex (PCx) of mammals (Stettler and Axel, 2009; Davison and Ehlers, 2011).

The selectivity of sensory representations can be modulated dynamically by changes in behavioral state, allowing an animal to learn and respond according to perceptual task. In mammals, the noradrenergic system originating in the locus coeruleus (LC) is implicated in signaling behavioral states such as attention, arousal and motivation (Sara, 2009; Sara and Bouret, 2012; Aston-Jones and Waterhouse, 2016). Noradrenergic modulation of the olfactory bulb enhances sensitivity of odor detection and discrimination, dependent on α-1-adrenergic receptors (Escanilla et al., 2010, 2012), and LC activation enhances the excitability of PCx pyramidal neurons (Bouret and Sara, 2002), and LC activation coincides with reward anticipation in appetitive odor discrimination (Bouret and Sara, 2004). However, the circuit and synaptic mechanisms of modulation by NA are not well understood.

In insects, octopamine (OA), chemically and functionally homologous to noradrenalin (NA) in mammals, can mediate changes in behavioral state that often promote activity, for example: sensitization of reflex actions in locust (Sombati and Hoyle, 1984); aggressive state in crickets (Stevenson et al., 2005); initiation and maintenance of flight state (Brembs et al., 2007; Suver et al. 2012); and enhanced excitability of *Drosophila* motion detection neurons during flight (Strother et al. 2018). Another potential role of OA is as a reward signal: although this role is at face value distinct from a role in promoting activity or preparedness, OA appears to encode unconditioned stimuli in honeybee (Hammer, 1993; Hammer and Menzel, 1998; Menzel 2012), cricket (Matsumoto et al. 2015), and *Drosophila* (Schwaertzel et al. 2003) appetitive learning paradigms. However, taken together, the OA system in insects is heavily involved in signaling behavioral states, comparable to NA in mammals.

Behavioral states facilitate the processing of visual sensory input associated to behavioral relevance (Gilbert and Li, 2013). At the circuit level, two models have been proposed, increase in response gain (Treue and Martinez Trujillo, 1999; Reynolds and Chelazzi, 2004), and changes in tuning properties of cortical visual neurons, reflecting sensory driven stimuli and behavioral context (Li et al. 2004). Although behavioral studies are extensive, the circuit and synaptic mechanisms of these signaling inputs are not well understood. We aimed to dissect the role of the OA circuitry in sensory processing. We used the simple sensory "cortex" of larval *Drosophila*, the calyx, which is the sensory input region of the mushroom bodies (MBs), the insect memory center. Here, each MB neuron (Kenyon cell, KC) typically arborizes in several glomeruli, most of which are organized around the terminus of an olfactory projection neuron (PN); KCs thus combinatorially integrate multiple sensory input channels (Masuda-Nakagawa et al., 2005; Eichler et al., 2017). Inhibitory feedback (Lin et al., 2014; Masuda-Nakagawa et al. 2014), helps to maintain KC sparse responses and odor selectivity (Honegger et al., 2011), analogous to inhibition in the mammalian PCx (Poo and Isaacson, 2009; Settler and Axel, 2009; Gire et al. 2013).

The larval MB calyx is also innervated by two OA neurons, sVUMmd1 and sVUMmx1, ventral unpaired medial neurons with dendritic fields originating in the mandibular and maxillary neuromeres respectively of the subesophageal zone (SEZ) (Selcho et al., 2014). These sVUM1 neurons also innervate the olfactory neuropiles of the antennal lobe (AL) and lateral horn. This pattern of innervation is conserved in other insects, for example by dorsal unpaired median (DUM) neurons in locust (Bräunig, 1991), the VUMmx1 neuron in honeybee (Hammer 1993; Schröter et al. 2007), and OA-VUMa2 neurons in adult *Drosophila* (Busch et al. 2009). It also resembles the NA innervation of mammalian forebrain by LC neurons originating in the brainstem. Therefore, the network organization and coding principles in the larval MB calyx appear widely conserved, but with few neurons and genetically tractable tools, it provides many advantages to understand how individual neurons are integrated to generate a concerted neural activity pattern.

We therefore characterized the innervation pattern and synaptic partners of OA neurons in the calyx, the localization of the OA receptor Oamb in the calyx circuit, and the impact of OA calyx innervation on sensory input activity, and on behavioral odor discrimination. We find that OA neurons innervate all the major classes of calyx neuron to some degree, although only a small fraction of KCs. Activating OA neurons can affect both PN activity, and odor discrimination during learning and memory, without affecting underlying olfactory learning and memory ability.

Our findings reveal a synaptic mechanism “gating” at the second synapse in the olfactory pathway, that has an impact on odor discrimination in learning.

Results

sVUM1 neurons in the calyx and their polarity.

Two OA neurons innervate throughout the calyx without obvious regional preference. The larval calyx is innervated by two classes of OA neurons, sVUMmd1, and sVUMmx1, originating from the mandibular and maxillary neuromeres, respectively, in the subesophageal zone (SEZ), and labeled by the *Tdc2-GAL4* line (Selcho et al. 2014). To visualize the innervation pattern of both sVUM1 neurons in the calyx together, we used the Multicolor FlpOut technique (Nern et al. 2015). Flies of genotype *pBPhsFlp2::PEST(attP3); HA_V5_FLAG_OLLAS* were crossed to flies of *Tdc2-Gal4*, and single cell clones were generated by heat shock. Each sVUM1 neuron ramified throughout the calyx, and we only ever found a single sVUMmd1 or sVUMmx1 neuron labeled. When both sVUM1 neurons were labeled, they ramified through the calyx in a non-overlapping pattern, without obvious regional preference (Fig. 1).

OA neurons are presynaptic in the calyx. To visualize the polarity of the calyx-innervating sVUM1 neurons, we used *Tdc2-GAL4* to express either plasma membrane, presynaptic or dendritic markers (Fig. 2). The sVUM1 projections visualized by the plasma membrane marker CD4::tdTom showed dense ramification throughout the calyx, with bouton-like enlargements among glomeruli and in the core of the calyx (Fig. 2A). These enlargements contained OA, and were therefore presynaptic boutons; we observed 89 ± 7 (n= 12) OA-positive boutons per calyx. The presynaptic nature of the *Tdc2-GAL4*-expressing calyx boutons was further supported by the localization of the presynaptic markers nSyb::GFP (Fig. 2A) and Syt::GFP (Fig. 2B) in puncta throughout the calyx in these neurons, prominently between glomeruli or in the non-glomerular core of the calyx. The dendritic marker DenMark::mCherry is not detectable in the calyx (Fig. 2B), although it is strongly localized in the SEZ region (Fig. 2C), which may include other Tdc2-GAL4-expressing neurons as well as the sVUM1 neurons.

Identifying calyx OA neuron partners by GRASP

To visualize synaptic contacts between sVUM1 neurons and other calyx neurons, we used *Tdc2-LexA*, along with *GAL4* lines expressing in other calyx neurons, to drive the expression of the GRASP constructs *LexAop-CD4::spGFP11 and UAS-CD4::spGFP1-10* (Fig. 3). We labeled olfactory PNs using *NP225-GAL4* (Tanaka et al., 2009), and KCs using *MB247-GAL4* (Zars et al. 2000). We also tested for GRASP between sVUM1 neurons and two other classes of extrinsic calyx neurons. First, we labeled the larval APL using *NP2361-GAL4* (Masuda-Nakagawa et al., 2014), Second, the “Odd” class of neurons shows dendritic arborizations

throughout the calyx, with presynaptic terminals in the vicinity of the MB lobes (Slater et al., 2015), and appear to be the same as those designated as MBON-a1 and MBON-a2 by Eichler et al (2017); we identified a *GAL4* line, *OK263-GAL4*, which expresses in these neurons.

GRASP fluorescence. We detected GRASP using GFP fluorescence as widely distributed puncta in the calyx, suggestive of specific synaptic connections, between the sVUM1 neurons on the one hand, and PNs, KCs, the Odd, and APL neurons on the other (Fig. 3A). These findings suggest that the sVUM1 neurons may form synapses with all the neuronal classes that innervate throughout the calyx: PNs, KCs, the APL, and Odd neurons.

To test whether GRASP signals represented synaptic contacts of the sVUM1 neurons, we also immunolabeled brains with anti-OA. GRASP signals were identified, using a criterion that each GRASP signal was observed in at least two consecutive confocal sections, and discounting occasional GFP-positive axonal tracts that were negative for OA.

OA termini synapse with PNs. Using *Tdc2-LexA* and *NP225-GAL4* to express the GRASP constructs, we found GRASP signal at 49±3% of 80±4 (n=5) OA-positive boutons. OA-positive GRASP signals (Fig. 3B) were found in the core of the calyx away from glomeruli, in interglomerular spaces, and along the periphery of glomeruli. They are likely contacts between sVUM1 termini and PN axons. Around 13.5% (n=5) of total GRASP signals did not overlap with OA, and we cannot conclude that these are synaptic contacts. However, PNs are commonly postsynaptic to the termini of sVUM1 neurons, on their axonal or presynaptic processes, making axon-axon synapses.

OA termini synapse with KCs in the calyx. Using *Tdc2-LexA* and *MB247-GAL4* to express the GRASP constructs, we found GRASP signals at 51 ± 4 % of 185 ± 34 (n=3) OA boutons (Fig. 3C).

OA termini synapse with Odd neurons in the calyx. Using *Tdc2-LexA* and *OK263-GAL4* to express the GRASP constructs, we found GRASP signals at 51 ± 0.3 % of 123 ± 4.2 (n=3) OA labeled boutons. There were OA spots that were apposed to GFP (Fig. 3D).

OA termini synapse with the APL. Using *Tdc2-LexA* and *NP2361-GAL4* to express the GRASP constructs, we found GRASP signal at 77±4% of 74±12 (n=4) OA terminals, indicating that

sVUM1 neurons are presynaptic to the larval APL. Most of these GRASP signals were found between glomeruli, and more abundant towards the ventral calyx (Fig. 3E top panels).

Around 28.3 ± 1 GFP signals, 32.8 % ± 2.6 (n=3) GRASP signals, did not overlap with OA, and therefore do not represent synapses of the sVUM1 neurons onto the APL. Some of these appear to be tracts that lead to OA positive spots, rather than the characteristic round shape of synaptic GRASP signals, and might therefore be due to proximity of the sVUM1 axons with APL axons. Others could be due to synapses of the APL onto OA neuron axons. GABA labeling of brains of the same genotype, showed some GABA termini in close proximity to GRASP (Fig. 3E, bottom panels), suggesting that some contacts between APL and sVUM1 neurons could potentially be inputs from APL terminals onto the sVUM1 neurons. Labeling of Tdc2-GAL4>mCD8::GFP calyces with anti-GABA also showed some apposition of sVUM1 boutons to GABAergic termini of the APL (Fig. 3F).

Single cell GRASP. While the above GRASP experiments reveal the partners of the sVUM1 neurons in the calyx, they do not reveal whether the sVUMmd1 and sVUMmx1 have different partners. We therefore performed single-cell GRASP to label the contacts of each sVUM1 randomly, using Brp::mCherry as a presynaptic marker to verify whether GRASP signals have a synaptic localization. We distinguished the two sVUM1 neurons by the positions of their cell bodies in the SEZ, using local neuropil landmarks revealed by anti-Dlg labelling (Fig. 4A), and using single cell clones, we could identify sVUMmd1 and sVUMmx1 individually (Fig. 4B).

GRASP signals were detected between the *odd*-expressing neurons and both sVUMmd1 and sVUMmx1 (Fig. 4C), and similarly between the larval APL, and both sVUMmd1 and sVUMmx1 (Fig. 4D). Compared to standard GRASP, single cell GRASP signals were fewer, but clearly present and overlapping with the presynaptic marker Brp::mCherry. (Fig. 4D). Therefore, at least as judged by the APL and Odd neurons, both sVUM1 neurons appeared to have similar targets in the calyx.

Localization of a genomic Oamb::GFP fusion in PN terminals in calyx

To further understand how and where OA might act in the calyx, we investigated the localization of OA receptors in the calyx. *Drosophila* has a number of OA receptor classes defined both by sequence comparisons and pharmacology. Octopamine receptor in mushroom bodies (Oamb, also known as Dmoa1A or CG3856), an ortholog of human α1-adrenergic receptor (Roeder et al., 2003; Bauknecht and Jékely, 2017), is enriched in the MBs (Han et al.,

1998). *Drosophila* also has three OctβR receptors, which stimulate cAMP levels (Maqueira et al., 2005, Balfanz et al., 2005).

To detect the expression and subcellular localization of Oamb, we used recombinase-mediated cassette exchange (RMCE) with a MiMIC insertion (Venken et al., 2011), *MI12417*, in the third coding-region intron of *Oamb*, to tag endogenous *Oamb* with an exonic *EGFP-FlAsH-StrepII-TEV-3xFlag* fusion (Supp Figs. 1-4). Insertion of an EGFP-encoding exon here should tag all known splice variants of the Oamb protein in their third cytoplasmic loop, downstream of transmembrane (TM) domain 5 (Supp. Fig. 5,6); this includes the alternative TM6-TM7 regions encoded by two alternative groups of C-terminal exons (Supp Figs 4-6). Therefore, a protein trap generated from the *MI12417* insertion will not disrupt any transmembrane domains.

Six recombinant *Oamb::EGFP* stocks were recovered with the EGFP-encoding exon inserted in the same orientation as the *Oamb* transcript (Supp Fig. 7). One of these was designated as *Mi{PT-GFSTF.1}Oamb*$^{MI12417\text{-}GFSTF.1}$*,* or *Oamb(MI12417)::EGFP.1* or *Oamb::EGFP* for short. Both the original *MI12417 MiMIC* insertion, and *Oamb(MI12417)::EGFP* stocks were homozygous infertile, as expected from the egg-laying defects of *Oamb* mutants (Deady and Sun, 2015), suggesting that the Oamb::EGFP fusion might not be a functional Oamb protein. However, Oamb::EGFP was localized to glomeruli in the larval calyx (Fig. 5), implying that the protein folded normally and was not degraded by the ER unfolded protein response. Expression of *UAS-RFP* in the olfactory PN line *NP225-GAL4* showed localization of Oamb::EGFP in all PN termini labeled with the GAL4 line, as well as in some calyx glomeruli not labeled by *NP225-GAL4*, which may be either sites of non-olfactory sensory input, or olfactory glomeruli not labeled by *NP225-GAL4* (Masuda-Nakagawa et al. 2010) (Fig. 5A). The restriction of Oamb::EGFP to specific glomeruli implies that it is unlikely to be expressed in KC dendrites in the calyx, which arborize through all glomeruli. We also found no overlap of Oamb::EGFP with GABAergic APL terminals in the calyx (Fig. 5B), implying that it was not expressed in the larval APL. *OK263-GAL4* calyx projections also showed little or no overlap with Oamb::EGFP (Fig. 5C), suggesting that Oamb is not expressed in the Odd neuron calyx dendrites.

We found no detectable localization of GFP-tagged DmOctβR receptors to the calyx (data not shown). Octβ1R::EGFP (*CG6919*) was expressed weakly in a few ventral and medial AL glomeruli, but was not detectable in the calyx. Octβ2R::EGFP (*CG6989*), was not detectable

in either the calyx or AL, although it was expressed in a number of adjacent cell bodies that did not colocalize with PNs as labeled by *NP225-GAL4* driving RFP expression. We could not detect any expression of Octβ3R::EGFP.

Stimulation of OA neurons enhances odor-evoked responses in calyx PN terminals.

Since Oamb is in the α1-adrenergic receptor family and activates release of Ca^{2+} from intracellular stores via Gq (Morita et al., 2006; Lee et al., 2009), we tested whether activation of OA neurons could increase odor-evoked responses in calyx PN terminals. We therefore measured calyx PN terminal responses, using *NP225-GAL4* and *UAS-JRCaMP1b*, in the presence of a *LexAop-ChR2(XXL)* construct either in the absence or presence of the OA driver line *Tdc2-LexA*. We measured responses in individual calyces, to (sequentially) (i) an odor pulse ("odor-only"); (ii) an odor pulse delivered 0.5 seconds after the end of a blue light pulse ("light+odor"); (iii) a pulse of blue light to activate ChR2(XXL) if expressed ("light-only"). We corrected the light+odor response first by subtracting any light-only response in that calyx, and second a "bleach correction" for fluorescence decay between the odor-only and odor+light responses in control larvae lacking *Tdc2-LexA*. In larvae lacking *Tdc2-LexA* (and hence lacking specific ChR2(XXL) expression, we found no significant effect of prior light exposure on odor-evoked responses; in the presence of *Tdc2-LexA*, to drive ChR2(XXL) expression in OA neurons, we found a small but significant enhancement of odor-evoked responses in PN calyx terminals (Fig. 6). Therefore we conclude that OA innervation of PNs can enhance their presynaptic evoked Ca^{2+} responses, and hence likely increase neurotransmitter release.

Activating an OA neuron subset including sVUM1 neurons impairs behavioral odor discrimination

Since the calyx is a site where MB neurons integrate sensory information that comprises conditioned stimuli (CS) in associative learning, we reasoned that modulating the processing of this information might affect the ability of the brain to discriminate among CSs while learning, but without affecting its underlying learning ability. In particular, increased activity of PN inputs to the calyx might reduce the ability of the calyx to discriminate among odors. Therefore, to test whether OA innervation of the calyx affected odor discrimination during learning, we developed an assay that could distinguish odor discrimination assay from learning ability (Fig. 7). The rationale of this assay was developed in the honeybee by Stopfer et al. (1997); molecularly similar odors are more difficult to discriminate than molecularly dissimilar odors, giving a measure of discriminability. In this case similar odor pairs are generated by varying the proportions of two dissimilar odors in two different odor mixes. By combining odor choice

with an appetitive learning paradigm (Scherer et al. 2003), we tested the effect on behavioral odor discrimination of optogenetic activation of OA neurons in third instar larvae, using the long-wavelength absorbing channelrhodopsin, CsChrimson (Klapoetke et al., 2013).

Since we did not have *GAL4* or *LexA* drivers completely specific for sVUM1 neurons, we used an intersectional approach to restrict the expression of CsChrimson to a small subset of OA neurons including the sVUM1 neurons. We could use *LexAop-FLP* and a *GAL80* cassette flanked by two *FRT* sites to express *UAS-CsChrimson* only in neurons that expressed both *GMR34A11-GAL4* (which labels some VUM neurons in addition to non-OA neurons), and *Tdc2-LexA*. We thus expressed CsChrimson in only five OA neurons in the SEZ of the larval brain: two (1.8 ± 0.39 (n=12)) in the mandibular neuromere (including sVUMmd1), two (2 ± 0.43 (n=12)) in the maxillary neuromere (including sVUMmx1), and one (1 ± 0 (n=12)) in the labial neuromere (Fig. 8). The second neuron labeled in each neuromere could be sVUM2 or sVUM3, however, sVUM1 neurons are the only neurons of this subset to innervate the AL and calyces.

Activation of these OA neurons, during conditioning but not during testing, had no effect on the ability of larvae to discriminate odors in an appetitive learning assay using a dissimilar odor pair, but abolished their ability to discriminate a similar odor pair, implying that odor discrimination is affected by activation of these neurons, but not underlying learning ability (Fig. 8).

Discussion

OA neurons target extrinsic neurons within the calyx circuitry

Two OA neurons originating in the SEZ, sVUMmd1 and sVUM mx1, innervate the same brain neuropiles, with postsynaptic processes in the SEZ and presynaptic processes in the antennal lobe and MB calyces (Fig. 2). Using GRASP, we found contacts of sVUM1 presynaptic terminals with KCs, PNs, Odd and APL neurons in the calyx, suggesting that sVUM1 neurons can potentially regulate these neurons. However, most KCs cannot be directly affected by sVUM1 innervation: the tens of contacts between the sVUM1 neurons and KCs is less than the 300-plus KCs present in third instar larvae (Pauls et al., 2010), and Eichler et al. (2017) also find inputs of either sVUM1 neuron (which they call OAN-a1 and OAN-a2) into fewer than 10-15% of KCs in first instar larvae. Therefore, context-dependent signaling by OA in the calyx must principally affect MB activity via its other input neurons, not by direct action on KC dendrites.

Connectomic analysis of a six-hour first-instar larva (Eichler et al. 2017) shows that the sVUM1 neurons, with only 36 active zones in a left brain, and 48 in a right brain, have a qualitatively similar but less extensive calyx innervation pattern than we observe in third instar, with 89 ± 7 [n=12] OA-positive boutons per calyx, and even more active zones, assuming multiple active zones per bouton. Consistent with our findings, Eichler et al (2017) also report substantial presynaptic contacts of sVUM1 neurons with Odd neuron dendrites, and some synapses of sVUM1 neurons with KCs, but not with most KCs; they do not comment on synapses with PNs or the APL.

OA modulation of PN activity

GRASP analyses suggest that PNs are postsynaptic to the sVUM1 neurons (Fig. 3). Indeed, an Oamb::eGFP exon-trap fusion is localized on PN presynaptic terminals, albeit more widely than GRASP puncta (Fig. 5). Similarly, the honeybee Oamb ortholog AmOA1 is found widely in the calyx (Sinakevitch et al., 2011), although these authors do not distinguish between PN terminals or KC dendrites. Much aminergic neurotransmission acts via extrasynaptic receptors (Bentley et al., 2016) and this may be the case for Oamb in PN terminals, Oamb is a GPCR that signals apparently through Gq, to release Ca^{2+} from intracellular stores (Balfanz et al., 2005; Morita et al, 2006); it may also elevate cAMP (Han et al., 1998), although this effect appears smaller (Balfanz et al., 2005). Consistent with this, optogenetic activation of sVUM1 neuron terminals in the calyx led to potentiation of odor-evoked [Ca^{2+}] in PN terminals (Fig. 6),

and should therefore enhance acetylcholine release from PN terminals. This effect could be serving as a gating mechanism to increase signal to noise ratio; at lower stimulus intensities this would facilitate the detection of subthreshold signals under behavioral states that promote OA release. Such a role for NA is also found in the mammalian olfactory bulb: here, LC input improves the detection of peri-threshold stimuli (Jiang et al., 1996), and facilitates the detection of near threshold odors, when rewarded (Escanilla et al., 2012), via an increase in mitral cell excitability mediated by NA action on α1-adrenergic receptor (Ciombor et al. 1999; Hayar et al. 2001). OA has comparable roles in the *Drosophila* central visual system, for example increasing the gain of motion-sensitive neurons in response to behavioral states such as walking or flight. (Chiappe et al. 2010; Maimon et al., 2010; Suver et al., 2012), sometimes via Ca^{2+} responses elicited by OA inputs in visual system neurons (Strother et al., 2018).

Roles of APL and Odd neurons in calyx activity

sVUM1 presynaptic termini also make many contacts with both the APL and Odd neurons (Fig. 3, 4). Odd neurons ramify throughout the calyx and receive input from PNs generally, thus forming a channel for non-selective odor processing that is parallel to the main MB odor-specific processing through KCs. A similar division of processing is seen in the visual pathway downstream of area V1, the primary sensory area in the cortex, with the segregation of the "what" pathway, for object recognition, from the dorsal "where" pathway that is involved in motion detection, visually guided movements and attentional control (Livingston and Hubel, 1988, Gilbert, 2013). sVUM1 neurons have extensive contacts with Odd neurons and could potentially change their gain or tuning properties, to signal changes in behavioural state that guide odor-driven choice behaviours. In fact Odd neurons have been implicated in chemotactic behaviour (Slater et al., 2015).

The APL mediates a negative feedback loop from KC outputs in the MB lobes to KC inputs in the calyx, thus potentially both limiting the duration of KC activity and improving their odor discrimination (Masuda-Nakagawa et al., 2014; Lin et al., 2014). sVUM1 synapses onto the APL in the calyx could therefore potentially regulate this feedback loop. This could increase signal-to-noise ratio, in a context-dependent manner, by sharpening odor representations in the calyx via APL inhibitory feedback, similar to the "gain control" mechanism with enhancement of behaviorally relevant responses and suppression of non-relevant ones, in monkey visual system, (Treue and Martinez Trujillo, 1999, Gilbert and Li, 2013). Similarly, songbirds possess a similar mechanism, with a gate open to the unique birdsong only during vocalization, in a behavioral state-dependent manner (Schmidt and Konishi, 1998). In addition,

since we observed some GRASP signals adjacent to GABA termini (Fig. 3E), APL feedback could also inhibit OA release from sVUM1 termini, further increasing the complexity of interactions between OA innervation and the KC/APL negative feedback loop. NA regulation of inhibitory neurons is also a feature of the mammalian olfactory circuitry. In olfactory bulb, disinhibition of mitral cell (equivalent to PN) activity by NA regulation of inhibitory granule cells has been proposed (Nai et al. 2009). In mammalian PCx, feedforward and feedback inhibition are postulated to enhance cortical representation of strong inputs (Stokes and Isaacson, 2010), and the PCx receives extensive NA innervation from the LC, although its role in modulating inhibition has not been investigated.

Odor discrimination learning

A role for OA as a reinforcer in appetitive associative learning has been shown in honeybees and flies. The honeybee VUMmx1 neuron has properties of a reinforcer; its depolarization could replace sugar reinforcement in appetitive learning (Hammer, 1993), and injection of OA into the MB calyx induced memory consolidation (Hammer and Menzel, 1998). Furthermore, increased density of calyx microglomeruli is observed in long term memory (Hourcade et al. 2010) and KC claws showed increased responses after appetitive conditioning (Szyszka et al. 2008). It has been proposed that VUMmx1 learns about the value of the odor, and acts as a prediction error signal in appetitive learning (Menzel, 2012). However, associative plasticity in the MBs in *Drosophila*, is thought to reside mainly in the lobes rather than the calyx, for both appetitive (Schwaertzel et al. 2003; Schroll et al. 2006; Liu et al. 2012) and aversive learning (Aso et al., 2012, 2014). OA as a reinforcer in appetitive learning appears to act via Oamb expressed in PAM dopamine neurons that target the MB lobes, and a set of OA neurons that includes OA-VUMa2, the equivalent of larval VUMmx1, did not induce and is not required for appetitive learning in adult *Drosophila* (Burke et al. 2012). Furthermore, Oamb is required in KCs for adult appetitive learning (Kim et al., 2013), suggesting some direct input of an OA-encoded appetitive signal into KCs. Taken together, OA action as a reinforcer in associative learning might occur via unidentified inputs into dopaminergic neurons or KC lobes – a separate role from gating selected sensory information, which is favored by our imaging and behavioral data, and is also suggested as a role of NA (Berridge and Waterhouse, 2003).

Here we observed that the discrimination of similar odors was compromised, in a reciprocal associative learning paradigm, by VUM1 activation. One explanation is that VUM1 activation enhanced the gain of stimulus-driven PNs, increasing the magnitude and number of KCs responding, and therefore representations by KCs of CS+ and CS- increased in overlap, and

lower discriminability of similar odors. Furthermore the effect was specific to the 5 neurons, including VUM1s targeted by our experiments.

Perspectives

Sensory representations are dynamically modified by higher brain signaling, according to behavioral state such as attention, expectation, and behavioral task; and LC (locus coeruleus) activation in mammals and OA activation in insects, correlate with changes in behavioral states. Mammalian olfactory neuropiles are densely innervated by noradrenergic input, similar to the dense octopaminergic sVUM1 neurons innervation of AL and calyx in insects. Although behavioral data is abundant, understanding of the circuit and synaptic mechanisms of NA/OA requires the identification of the synapses and receptors that they target. The innervation of sVUM1 neurons throughout the calyx, and their potential synaptic connections to PNs, KCs, APL, and odd-like neurons, suggest that OA induces a network level switch both via gating input afferent activity, and by interacting with the KC/APL feedback loop, and thus also affecting the output activity from the calyx – not only through KCs but also potentially via the Odd neurons. Behavioral demands would determine the balance between sensitivity and discrimination via OA; whether to escape from a predator at all cost, or the need to recognize closely similar smells associated to food or danger. The effect of brain signals on sensitivity and discrimination is also observed in the human brain; in hallucinations in schizophrenia (Dierks 1999). NA/OA are teaching signals downstream higher order brain commands that compute cognitive processes, future work is necessary to understand the circuits upstream NA/OA and how they regulate the dynamics of bottom-up sensory circuits.

Materials and Methods:

Genetics and molecular biology.

Fly Stocks. Flies were raised on standard cornmeal medium at 25°C and subjected to a 12 hour day/night cycle. Stocks used are listed in Table 1.

MultiColor FlpOut. MultiColor FlpOut was performed according to Nern et al. (2015). Females of genotype *pBPhsFlp2::PEST(attP3); +; HA_V5_FLAG_OLLAS* ("MCFO-2") were crossed with male *Tdc2-Gal4* flies. Parents were left in vials to lay eggs for 24-hour intervals. After another 24 hours, larval progeny were heat shocked at 35-37°C by immersion in a heated circulated waterbath for 15-30 minutes, thus ensuring larvae were aged 24-48 hours after egg-laying (AEL) at the time of heat shock.

GRASP. Standard GRASP was according to Gordon and Scott (2009). Reconstituted GFP was detected using rat monoclonal anti-GFP. This did not detect either of the GRASP components GFP1-10 or GFP11, when *Gal4* or *LexA* drivers were used alone. GRASP signals had to meet a criterion of occurring in two consecutive 0.5-µm confocal sections. For single cell GRASP (Karuppudurai et al., 2014), we generated larvae carrying *P{hsFLP}*12, appropriate *GAL4* and *LexA* combinations, and a recombinant chromosome with insertions *LexAOp2-IVS>stop>spGFP11::CD4::HA-T2A-Brp::mCherry (attP2), UAS-spGFP1-10::CD4,* and *UAS- HRP::CD2.* To generate labelled single cells, parents were allowed to lay eggs initially for 24-hour intervals, then for 6-hour intervals in vials containing half the amount of food. At 0-24h, 24-48h, or later at 12-18 h, 18-24 h, or 24-30 h AEL, progeny were heat shocked as above for 10-50 minutes at 37℃. Progeny were incubated from RT until dissection of non-tubby wandering third instar larvae.

Generation of an EGFP-tagged Oamb line. The *Mi{MIC}Oamb*^{MI12417} insertion in coding intron 3 of *Oamb* at 3R:20697059, (BDSC 57940; henceforth referred to as *MI12417*) was verified by PCR using primers *MI12417-5F/MiMIC-5R1* for the 5' end and *MI12417-3R/MiMIC-3F1* for the 3' end (Table 2; Supplementary Fig. 1). Sequencing of these PCR products and alignment with the *Drosophila* genome sequence using BLASTN (Altschul et al., 1990; https://blast.ncbi.nlm.nih.gov/) showed insertion of *MiMIC* at the recorded site of 3R 20697058-9 (Supplementary Figs. 2,3). The location of the *MI12417* insertion site relative to *Oamb* coding exons was determined by using Oamb-B sequences for BLASTN and TBLASTN queries of the *Drosophila* genome assembly (http://flybase.org/blast/; Supplementary Fig. 4). TMHMM

(Sonnhammer et al., 1998; http://www.cbs.dtu.dk/services/TMHMM/) was used to predict the amino-acid coordinates of Oamb transmembrane (TM) domains (Supplementary Figs. 5,6).

To insert an EGFP-encoding exon into the *MI12417* insertion by RMCE, we chose the splice phase-1 version of *EGFP-FlAsH-StrepII-TEV-3xFlag* plasmid (DGRC 1306; Venken et al., 2011) as recommended by the Baylor Gene Disruption Project (http://flypush.imgen.bcm.tmc.edu/pscreen/rmce/rmce.php?entry=RM00888). This was co-injected with a helper phiC31-integrase plasmid (Venken et al., 2011) by the *Drosophila* microinjection facility (Department of Genetics, University of Cambridge). Injected embryos were left to hatch into adult flies and crossed to a *y w* double balancer stock. RMCE events were identified by loss of the *MiMIC yellow*$^{+}$ marker in F1 progeny. Four PCR reactions were carried out to determine the orientation of the EGFP cassette in each recombinant *Oamb::EGFP* stock (Table 2) as described in Venken et al. (2011).

***OctβR* EGFP fusions.** For *Octβ1R* and *Octβ3R*, we used lines *Octβ1R*$^{MI05807\text{-}GFSTF.2}$ and *Octβ3R*$^{MI06217\text{-}GFSTF.1}$ (Bloomington stocks 60236 and 60245), respectively, as *Octβ1R::EGFP* and *Octβ3::EGFP* exon traps. For *Octβ2R*, we used *Mi{MIC}Octβ2R*^{MI13416} to generate *Octβ2R*$^{MI13416\text{-}GFSTF.2}$ using a similar approach as that described above for Oamb::EGFP. We also generated a second *Octβ3::EGFP* exon trap, *Octβ3R*$^{MI06217\text{-}GFSTF.0}$, in a different reading frame from Bloomington stock 60245 , to allow for the possibility of the *EGFP* exon being spliced as in transcripts *RJ* or *RK* (frame 0, with only *RJ* able to encode all seven TM domains), rather than *RF* or *RG* (frame 1). Positions of each insertion were confirmed by PCR and sequencing similarly to Oamb, using primers as described in Table 2.

Molecular methods. Genomic DNA was extracted from 15-30 flies (1-7 days after eclosion) and homogenized in 100 mM Tris-HCl, 8.5; 80 mM NaCl, (Sigma 31434); 5% Sucrose (Sigma S0389); 0.5% SDS (Sigma L4509); 50 mM Na-EDTA (Sigma ED2SS), pH 8.0. The homogenate was incubated with RNase A (Roche 10109142001) for 1 hour at 37°C followed by Proteinase K (Roche 03115887001) for 1 hour at 50°C, and purified with phenol-chloroform (Sigma 77617) and chloroform (Sigma C2432). DNA was precipitated with 0.6 volumes of isopropanol (Sigma, 59304) and washed with 75% ethanol (Sigma E7023), dried overnight at room temperature and re-suspended in 10 mM Tris-HCl pH 8.0 (Sigma T6066).

PCR reactions (20 µl) contained 0.4 µl or 1 µl genomic DNA, 1 µl of each 10 µM primer (Sigma), 2µl of 10X PCR buffer (Qiagen 203203), 0.4 µl of 10 µM dNTP mix (Roche 11581295001),

0.08 µl of 5 U/µl HotStarTaq DNA polymerase (Qiagen 203203) and 15.1 µl or 14.5 µl milliQ water. PCR cycling in a G-Storm Thermal Cycler (GS4) was: 15 minutes at 95°C; 40 cycles of: denaturation at 94°C for 30s, annealing at 60°C for 30s and elongation at 72°C for 1 min; and a final elongation step at 72°C for 10 minutes. PCR products were loaded with 6X DNA gel-loading dye (ThermoFisher R0611) on a 1% Agarose Gel (LifeTech 16500500; 1X TBE buffer, LifeTech 16500500) with GelRed (Biotium 41003-T) for gel electrophoresis. 100 bp DNA ladder was used as a marker (LifeTech 15628019). PCR products were purified using the Qiaquick PCR Purification Kit (Qiagen, 28104), and sequenced at the Department of Biochemistry Sequencing Facility (University of Cambridge).

Immunohistochemistry and Confocal imaging.

Third instar wandering larval brains (144-176 hours AEL) were dissected in cold PBS (Sigma P4417), fixed in 4% Formaldehyde (Polysciences 18814) / PEM buffer (0.1 M PIPES, Sigma P1851; 2 mM EGTA, Sigma E3889; 1 mM $MgSO_4$; NaOH) for 2 hours at 4°C, washed for 3x10 minutes (or 4x15 minutes) in 0.3% Triton-X (Sigma T8787) in PBS (PBT) and incubated in 10% NGS (Normal goat serum; Vector Labs S-1000) in 0.3% PBT for 1 hour at room temperature. Brains were incubated in primary antibody in 10% NGS-0.3% PBT at 4°C for 2-3 days on a mini disk rotor (Biocraft, BC-710), washed for 3x15 minutes with 0.3% PBT and further incubated in secondary antibody in 10% NGS at 4°C for 2-3 days again on the mini disk rotor. Brains were finally washed 1x15 minutes with PBT, followed by 3x10 minutes with PBS, and left in 50% Glycerol/PBS at 4°C for at least one overnight prior to imaging.

Primary and secondary antibodies are listed in Table 3. Brains were incubated in primary antibody at 4°C for 2-3 nights, washed three times in PBT for 15-minutes, and incubated in secondary antibody for 2-3 more nights. To reduce background with the polyclonal chicken anti-GFP (Abcam, Ab13970), it was pre-incubated with *MI12417* larval brains which do not express GFP. Fifty *MI12417* larval brains were incubated in 1:20 chicken anti-GFP in 10% NGS in 0.3% PBT at 4°C for overnight. A further 50 *MI12417* larval brains were added and further incubated at 4°C over 2 nights. Mounting and orientation of brains for image acquisition was as described in supplemental information in Masuda-Nakagawa et al. (2009). Imaging was carried out using a Zeiss LSM710 Confocal Microscope with a 40X NA1.3 oil objective. Images were processed using ImageJ software (https://imagej.nih.gov/ij/download.html).

Optogenetics and live imaging.

All crosses were performed on cornmeal-yeast-agar medium supplemented with 100 µM all-trans-Retinal (Sigma, R2500). Crosses were kept at 23°C in the dark wrapped in tinfoil, and when necessary handled under dim amber light (591 nm).

Combined optogenetics and activity imaging was performed by crossing *LexAop-ChR2-XXL; UAS-jRCaMP1b/TM6B* virgin females to stocks expressing relevant *GAL4* and LexA insertions. ChR2-XXL function was confirmed by crossing these females to *nSyb-LexA/CyO::GFP* males and testing undissected, non-*CyO::GFP* larval progeny for light-induced body contraction under imaging conditions. Driver expression in all *GAL4* and *LexA* combination lines was tested by imaging RFP and GFP expression in the larval progeny of a cross between males of each line to virgin females of a *UAS-RFP LexAop-GFP* double reporter line (Bloomington stock 32229). As a positive control, virgins of genotype *LexAop-ChR2-XXL; UAS-jRCaMP1b/TM6B* were crossed either to *NP2631-GAL4; MB247-LexA/TM6B* to activate KCs and image APL responses, or to *NP2631-GAL4* males as a negative control. To activate OA neurons and image PNs, *LexAop-ChR2-XXL; UAS-jRCaMP1b/TM6B* virgins were crossed to *NP225-GAL4; Tdc2-LexA/TM6B* males, or to *NP225-GAL4; MKRS/TM6B* males as a negative control, and only non-*TM6B* (non-*Tb*) larvae were imaged.

Humidified odors were presented through valves controlled by a Master-8-cp controller (AMPI, Jerusalem, Israel) as described (Masuda-Nakagawa et al., 2009). The concentration of EA (Ethyl Acetate) was reduced to 1/10,000 so that only a 1-3 PN terminals in the calyx responded to a 2-second odor presentation in any given optical slice.

Wandering stage L3 *Drosophila* were dissected and mounted for imaging as previously described (Masuda-Nakagawa et al., 2009) under an Olympus BX50-WI microscope with a Zeiss W Plan-Apochromat 40x/1.0 DIC M27 objective. Dissection was performed under dim amber (591 nm) light and the condenser light of the BX50-WI was passed through an ET632/60 M emission filter. A 470nm LED filtered through a ET470/40x (Chroma, VT, USA) emission filter and regulated by a Dual LED Power Supply (Cairn Research, Faversham, UK) was used to illuminate the sample through the objective via a Cairn OptoLED LED mount (Cairn Research) onto the Olympus BX50-WI BX-FLA vertical illuminator. The vertical illuminator aperture was minimized to a diameter of approximately twice that of the calyx (from a dorsal view) and centered within the camera's field of view. A T495lpxr dichroic mirror (Chroma, VT, USA) directed the LED onto the sample while preventing 470nm light reflected off the sample from reaching the microscope output. The Dual LED intensity was set at the minimum value

that reliably evoked contractions in the body wall of mounted *LexAop-ChR2-XXL/nSyb-LexA; UAS-jRCaMP1b/+* larvae.

jRCaMP1b fluorescence was imaged using an Andor iXon+ DU-888E-CO-#BV EM-CCD camera (Andor, Belfast, UK) attached to a CSU22 spinning disc confocal (Yokogawa Electric Corporation) via a Cairn Research Optosplit II (Faversham, UK), all mounted on the above Olympus BX50-WI. A 561nm excitation laser was used for all imaging, at 20% laser power; at this power, *LexAop-ChR2-XXL/nSyb-LexA; UAS-jRCaMP1b/ MKRS* larvae showed no movement in response to the laser. The room was kept at 23°C. The Master-8-cp controller synchronized the timing of imaging, LED illumination, and odor delivery, while images were recorded using Micro-Manager (Edelstein et al., 2010).

To image the effect of OA neuron depolarization on odor-evoked responses of PN axon termini, we identified either the left or right calyx of each brain and centered it within the field of view. All preparations were left to settle for at least two minutes before experiments began, and any still moving at 15 minutes were discarded. We performed four sequential imaging paradigms on each preparation; each acquisition lasted 12 seconds at 5 frames per second with a 100-ms exposure time, with a gap of at least 30 seconds between acquisitions. The first paradigm was an odor-only control, a 2-second odor pulse presented after 4 seconds. If no response was found, we repeated the presentation on a different z-section of the calyx. If no response was observed after 4 attempts, we discarded the preparation. The second paradigm was light+odor; we first presented a 2-second light pulse from the 470nm LED after 1.5 seconds, and then presented odor as in the first paradigm, i.e. 0.5 seconds after the end of the 2-second light pulse. Calyx glomeruli were used as landmarks to refocus as necessary. The third paradigm was a light-only control, delivered as in paradigm 2. The fourth and final paradigm was the same as the first, to control for preparation degradation over time; if no odor response was observed, the preparation was discarded.

To quantify activity in PN terminals, the experimenter was blinded to the genotype of each time-series of images. Each image of each time series was motion corrected using the moco plugin (Dubbs et al., 2016). Regions of interest (ROIs) for the best responding glomerulus in the odor-only paradigm (judged by eye during acquisition), and for background fluorescence outside the calyx, were drawn manually on the frame with peak fluorescence. In each consecutive imaging paradigm, the ROI was redrawn around the glomerulus to compensate for drift of the preparation. The average intensity for each ROI was calculated from each frame,

and background fluorescence was subtracted . Each acquisition consisted of 60 frames of background-subtracted intensity data acquired over 12 seconds. To smoothen out frame-to-frame variation, we used the overlapping moving averages of three sequential frames, leaving 58 frames of smoothed data.

To determine the effect of OA neuron activation on PN terminal activity, we performed two comparisons: the first was a control comparison, of odor-evoked PN responses in the absence (Paradigm 1) or presence (Paradigm 2) of prior optogenetic activation of OA neurons, in control brains of genotype *LexAop-ChR2-XXL/ NP225-GAL4; UAS-jRCaMP1b/ MKRS*. The second comparison was similar, but in brains of *LexAop-ChR2-XXL/ NP225-GAL4; UAS-jRCaMP1b/ Tdc2-LexA*, in which ChR2-XXL expression is targeted to OA neurons. To calculate the odor-evoked response to OA neuron activation, we applied two corrections to the Light+Odor response (Paradigm 2): we first subtracted the Light-Only response in the same brain (Paradigm 3); we then applied a bleach correction factor to each timepoint in each preparation, since the maximal responses were slightly lower in Paradigm 3 than in Paradigm 1. The bleach correction factor was calculated by (i) averaging the responses for each frame, from all preparations in the odor-only (paradigm 1) and light+odor (paradigm 2) responses; (ii) summing these averaged responses from the start of the odor pulse (frame 21) until the end of the acquisition (frame 59), to obtain a measure of the total strength of the response over the acquisition period; (iii) dividing the summed average response for odor-only by the summed average response for light+odor, to achieve a correction factor of 1.103. The timecourse of average responses in the absence and presence of light matched closely for the control larval genotype, but light activation give responses that were higher than without light consistently across the whole timecourse of the odor response. After corrections, we measured the total evoked response of each calyx, integrated over 6 seconds from the end of the odor pulse to the end of the acquisition, and assayed the effect of OA neuron activation in each individual calyx by comparing responses between the absence (paradigm 1) and presence (paradigm 3, corrected as above) of light. We used Prism (Graphpad Software, San Diego, CA, USA) to generate graphs, and to perform non-parametric Wilcoxon matched-pairs signed rank tests to compare the two conditions within control calyces lacking *Tdc2-LexA*, and again compare the two conditions within calyces expressing *ChR2-XXL* under control of *Tdc2-LexA*. Representative panels for display were chosen so that the difference between corrected “light+odor” and “odor-only” responses was close to the median value, and to have visually similar resting fluorescence levels.

Behavioral assay.

Larval culture. Males of genotype *w; Tdc2-LexA; GMR34A11-GAL4/TM6B* were crossed to females of genotype *Tub84B(FRT-GAL80)1, w; LexAop-FLP; UAS-Chrimson::mVenus/TM6B* to generate F1 larvae in which *UAS-Chrimson::mVenus* could be expressed only in cells expressing both *Tdc2-LexA* and *GMR34A11-GAL4*, in which LexA-dependent *FLP* expression had removed the GAL4 inhibitor GAL80. Larvae were allowed to develop in food vials containing 100 µM all-trans-retinal, in the dark at 21 degrees. For both the retinal and non-retinal food vials, transfer of adults into new vials happens both in the morning and in the evening, to then collect them after 108-120 hours in the case of non-retinal vials at 25°C, and after 132-144 hours for those kept in retinal vials at 23°C.

Behavioral arena. Agarose petri dishes were prepared the day before use, by using 100 ml of distilled water with 0.9% agarose (Sigma A9539). Fructose petri dishes were prepared similarly, but containing 35% fructose (Sigma-47740). Petri dishes had perforated lids, to facilitate creation of odorant gradients within the dish, by sucking air from a benchtop fume extractor (Sentry Air Systems (SAS), SS-200-WSL) at the back of the assay platform. Odorants were diluted in 10-µl volumes of paraffin oil (Sigma-Aldrich 76235), held in custom-built Teflon containers with pierced lids (7 holes), on the surface of agarose plates.

Light apparatus. The light apparatus contained a BK Precision pulse generator attached to a DC power pack, driving amber light LEDs (591 nm), constructed as described by deVries and Clandinin (2013), by the Psychology Department workshop of the University of Cambridge. One cycle of pulses consisted of 10-ms pulses at 10Hz for 30s, followed by 30s without pulses. This cycle was repeated 5 times, making a conditioning step of 5 minutes. This pulse frequency and width were chosen to replicate the activity of the only recorded sVUM1 neuron, the honeybee sVUMmx1, when activated by a sucrose reward (Hammer et al., 1993).

Behavior conditioning. Third-instar larvae were collected from vials using a metal sieve, and washed with tap water. Larvae were washed twice by transferring through a drop of water, and then placed on the conditioning agarose plate (35% fructose). A Teflon container with 10 µl of odor A to be reinforced was placed on the left side, and another containing paraffin oil (neutral) symmetrically on the right side, at positions marked on a black background, used to facilitate visualization of the larvae (Fig. 7). Larvae were conditioned on the fructose plate with odor A for 5 minutes under weak blue light. Larvae were then transferred to a water droplet using a brush, and again to a second water droplet to ensure no fructose traces remained, and then

to an agarose plate lacking fructose, on which a Teflon container with 10 µl of odor B (non-reinforced) was placed on the left side and a container with paraffin oil (neutral) on the right side. Larvae were conditioned for 5 minutes under weak blue light as above. This conditioning procedure on both plates was repeated for three cycles. For experiments using activation of OA neurons, the entire conditioning cycles were carried out under amber light (Fig. 7).

Odor dilutions. To avoid bias based on innate preferences of odors, odor concentrations were balanced to achieve a response index of around zero. Dilutions of ethyl acetate (EA) at 1:2000 and pentyl acetate (PA) at 1:500 were used. The dissimilar odor pair was ethyl acetate (EA) (Sigma-Aldrich, cat no. 319902) diluted 1:2000, and pentyl acetate (PA) (Sigma-Aldrich, cat no. 109584) diluted 1:500. The similar odor pair was mixtures of EA and PA at dilutions of 1:2000, and 1:500, respectively, at proportions of 1:4 EA:PA, and 4:1 of EA:PA.

Testing. Larvae were tested by placing them on an agarose plate carrying a container with odor A on one side, and a container with odor B on the other. Test was under blue light for 5 minutes. Larvae were counted on the side of odor A (conditioned), odor B (unconditioned) or in the neutral zone in the middle. In some experiments, larvae were transferred during the above procedures under white fluorescent ceiling lighting rather than weak blue light, but we detected no difference in learning scores between these conditions using ANOVA, as described in the Results section. Performance Index (PI) was calculated as:

$$PI = (N_{conditioned} - N_{unconditioned}) / N_{total}$$

$N_{conditioned}$: larvae on the side of the conditioned odor.

$N_{unconditioned}$: larvae on the side of the unconditioned odor.

N_{Total}: larvae on the side of conditioned odor, unconditioned odor, and middle zone.

Learning Index (LI) was calculated after both a conditioning with odor A and a reciprocal conditioning with odor B (with a different sample of larvae), using the formula:

$$LI = (PI_A - PI_B)/2$$

Statistical analysis. Planned comparisons were performed using t-tests. A four-factor ANOVA using SPSS software was used to test whether learning index was affected by food type (retinal vs. non-retinal), light (blue vs. amber), odor pairs (similar pair vs. dissimilar pair), or experimenter (either of two).

Acknowledgements:

We thank T. Awasaki, S. Certel, K. Ito, M Landgraf, T. Lee, C.H.-Lee, B Pfeiffer, M. Ramaswami, K. Scott, J Truman, and the Bloomington Drosophila Stock Center (BDSC) for numerous fly stocks, and the Developmental Studies Hybridoma Bank (DSHB), University of Iowa, for antibodies. We thank Tom Bland for helping set up the larval behavior assay, and M Morgan for help in building optogenetic illumination apparatus.

JYHW was supported by a Medical Research Council studentship and MM was supported by a UK Genetics Society “Genes and Development” summer scholarship and an award from the Bedford Fund, King’s College Cambridge. This work was supported by BBSRC Grants BB/I022651/1 and BB/N007948/1 and an Isaac Newton Trust award to LMM-N and CJO’K.

Author contributions:

Experimental design: LMMN, CJO’K

Performed experiments: LMMN, ADM, BAW, JYHW, MM, SWZ.

Data analysis: LMMN, CJO’K, ADM, BAW.

Paper writing: LMMN

Paper editing: CJO’K

References

1. Altschul, S.F., Gish, W., Miller, W., Myers, E.W., and Lipman, D.J. (1990). Basic local alignment search tool. J. Mol. Biol. *215*, 403–410.
2. Aso, Y., Herb, A., Ogueta, M., Siwanowicz, I., Templier, T., Friedrich, A..B., Ito, K., Scholz, H., and Tanimoto, H. (2012). Three dopamine pathways induce aversive odor memories with different stability. PLoS Genet *8*:e1002768.
3. Aso, Y., Sitaraman, D., Ichinose, T., Kaun, K.R., Vogt, K., Belliart-Guérin, G., Plaçais, P.-Y., Robie, A.A., Yamagata, N., Schnaitmann, C., et al. (2014). Mushroom body output neurons encode valence and guide memory-based action selection in *Drosophila*. eLife *3*, e04580.
4. Aston-Jones, G., and Waterhouse, B. (2016) The locus coeruleus: from global projection system to adaptive regulation of behavior. Brain Res. *1645*, 75-78.
5. Balfanz, S., Strünker, T., Frings, S., and Baumann, A. (2005). A family of octopamine receptors that specifically induce cyclic AMP production or Ca2+ release in Drosophila melanogaster. J. Neurochem. *93*, 440–451.
6. Bauknecht, P., and Jékely, G. (2017). Ancient co-existence of norepinephrine, tyramine, and octopamine signaling in bilaterians. BMC Biology *15*, 6.
7. Bentley, B., Branicky, R., Barnes, C.L., Chew, Y.L., Yemini, E., Bullmore, E.T., Vértes, P.E., and Schafer, W.R. (2016) The Multilayer Connectome of *Caenorhabditis elegans*. PLoS Comput Biol *12*, e1005283.
8. Berridge, C.W., and Waterhouse, B.D. (2003). The locus coeruleus-noradrenergic system: modulation of behavioral state and state-dependent cognitive processes. Brain Res. Revs. *42*, 33-84.
9. Bouret, S., and Sara, S.J. (2002) Locus coeruleus activation modulates firing rate and temporal organization of odor-induced single-cell responses in rat piriform cortex. Eur. J. Neurosci. *16*, 2371-2382.
10. Bouret, S., and Sara, S.J. (2004) Reward expectation, orientation of attention, and locus coeruleus-medial frontal cortex interplay during learning. Eur. J. Neurosci. *20*, 791-802.
11. Braun, G., and Bicker, G. (1992). Habituation of an appetitive reflex in the honeybee. J. Neurophysiol. *67*, 588-598.
12. Bräunig, P. (1991). Suboesophageal DUM neurones innervate the principal neuropiles of the locust brain. Philos Trans R Soc Lond Biol *332*, 221–240.
13. Brembs, B., Christiansen, F., Pflüger, H.J., and Duch, C. (2007). Flight initiation and maintenance deficits in flies with genetically altered biogenic amine levels. J. Neurosci. 27, 11122-11131.
14. Burke, C.J., Huetteroth, W., Owald, D., Perisse, E., Krashes, M.J., Das, G., Gohl, D., Silies,

M., Certel, S., and Waddell, S. (2012). Layered reward signalling through octopamine and dopamine in *Drosophila*. Nature *492*, 433–437.

15. Busch, S., Selcho, M., Ito, K., and Tanimoto, H. (2009). A map of octopaminergic neurons in the *Drosophila* brain. J. Comp. Neurol., *513*, 643-667.
16. Chiappe M.E., Seelig J.D., Reiser M.B., and Jayaraman V. (2010) Walking modulates speed sensitivity in *Drosophila* motion vision. Curr Biol *20*, 1470–1475.
17. Ciombor, K.J., Ennis, M, and Shipley, M.T. (1999). Norepinephrine increases rat mitral cell excitatory responses to weak olfactory nerve input via alpha-1 receptors in vitro. Neurosci. *90*, 595-606.
18. Cole, S.H., Carney, G.E., McClung, C.A., Willard, S.S., Taylor, B.J., and Hirsh, J. (2005. Two functional but noncomplementing *Drosophila* tyrosine decarboxylase genes. J. Biol. Chem. *280*, 14948-14955.
19. Dana, H., Mohar, B., Sun, Y., Narayan, S., Gordus, A., Hasseman, J.P., Tsegaye, G., Holt, G.T., Hu, A., Walpita, D., et al. (2016). Sensitive red protein calcium indicators for imaging neural activity. eLife *5*, e12727.
20. Davison, I.G., and Ehlers, M.D. (2011). Neural circuit mechanisms for pattern detection and feature combination in olfactory cortex. Neuron *70*, 82-94.
21. Deady, L.D., and Sun, J. (2015). A Follicle Rupture Assay Reveals an Essential Role for Follicular Adrenergic Signaling in *Drosophila* Ovulation. PLoS Genet. *11*, 1–21.
22. Dubbs, A., Guevara, J., and Yuste, R. (2016). moco: Fast motion correction for calcium imaging. Front. Neuroinform. *10*, 6.
23. Eichler, K., Li, F., Litwin-Kumar, A., Park, Y., Andrade, I., Schneider-Mizell, C.M., Saumweber, T., Huser, A., Eschbach, C., Gerber, B., et al.. (2017). The complete connectome of a learning and memory center in an insect brain. Nature *548*, 175-182.
24. Escanilla, O., Arrellanos, A., Karnow, A., Ennis, M., and Linster, C. (2010). Noradrenergic modulation of bahavioral odor detection and discrimination thresholds in the olfactory bulb. Eur J Neurosci. *32*, 458-468.
25. Escanilla, O., Alperin, S., Youssef, M., Ennis, M., and Linster, C. (2012). Noradrenergic but not cholinergic modulation of olfactory bulb during processing of near threshold concentration stimuli. Behav. Neurosci. *126*, 720-728.
26. Estes, P.S., Ho, G.L.Y., Narayanan, R., and Ramaswami, M. (2000). Synaptic localization and restricted diffusion of a *Drosophila* neuronal synaptobrevin - green fluorescent protein chimera in vivo. J. Neurogenet. *13*, 233-255.
27. Gilbert, C.D., and Li, W. (2013). Top-down influences on visual processing. Nature Revs. *14*, 350-363.

28. Gire, D.J., Restrepo, D., Sejmowski, T.J., Greer, C., De Carlos, J.A., and Lopez-Mascaraque, L. (2013). Temporal processing in the olfactory system: can we see a smell? Neuron *78*, 416-432.
29. Gordon, M. D., and Scott, K. (2009). Motor control in a *Drosophila* taste circuit. Neuron *61*, 373-384.
30. Gottfried, J.A. (2009). Function follows form: ecological constraints on odor codes and olfactory percepts. Curr. Opin. Neurobiol. *19*, 422-429.
31. Hammer, M. (1993). An identified neuron mediates the unconditioned stimulus in associative olfactory learning in honeybees. Nature *366*, 59-63.
32. Hammer, M. and Menzel, R. (1998). Multiple sites of associative odor learning as revealed by local brain injections of octopamine in honeybees. Learn. Mem. *5*, 146-156.
33. Han, K. A, Millar, N.S., and Davis, R.L. (1998). A novel octopamine receptor with preferential expression in *Drosophila* mushroom bodies. J. Neurosci. *18*, 3650–3658.
34. Han, C., Jan, L.Y., and Jan, Y.-N. (2011). Enhancer-driven membrane markers for analysis of nonautonomous mechanisms reveal neuron-glia interactions in *Drosophila*. Proc. Natl. Acad. Sci. USA *108*, 9673-9678.
35. Hayar, A., Heyward, P.M., Heinbockel, T., Shipley, M.T., and Ennis, M. (2001). Direct excitation of mitral cells via activation of alpha-1noradrenergic receptors in rat olfactory bulb slices. J. Neurophysiol. *86*, 2173-2182.
36. Honegger, K.S., Campbell, R.A.A., and Turner, G.C. (2011). Cellular-resolution population imaging reveals robust sparse coding in the *Drosophila* mushroom body. J. Neurosci. *31*, 11772-11785.
37. Hourcade, B., Muenz, T.S., Sandoz, J-C., Rossler, W., and Devaud, J-M. (2010). Long-term memory leads to synaptic reorganization in the mushroom bodies: a memory trace in the insect brain? J. Neurosci. *30*, 6461-6465.
38. Jenett, A., Rubin, G.M., Ngo, T.-T.B., Shepherd, D., Murphy, C., Dionne, H., Pfeiffer, B.D., Cavallaro, A., Hall, D., Jeter, J., et al. (2012). A GAL4-driver line resource for *Drosophila* neurobiology. Cell Reps. *2*, 991-1001.
39. Jiang, M., Griff, E.R., Ennis, M., Zimmer, L.A., and Shipley, M.T. (1996). Activation of Locus Coeruleus enhances the responses of olfactory bulb mitral cells to weak olfactory nerve input. J. Neurosci. *16*, 6319-6329.
40. Karuppudurai, T., Lin, T.-Y., Ting, C.-Y., Pursley, R., Melnattur, K. V., Diao, F., White, B. H., Macpherson, L. J., Gallio, M., Pohida, T., and Lee, C.-H. (2014). A hard-wired glutamatergic circuit pools and relays UV signals to mediate spectral preference in *Drosophila*. Neuron *81*, 603-615.

41. Kim, Y.-C., Lee, H.-G., Lim, J., and Han, K.-A. (2013). Appetitive learning requires the alpha1-like octopamine receptor OAMB in the *Drosophila* mushroom body neurons. J. Neurosci. *33*, 1672–1677.
42. Klapoetke, N. C., Mutata, Y., Kim, S.S., Pulver, S.R., Birdsey-Benson, A., Cho, Y.K., Morimoto, T.K., Chuong, A.S., Carpenter, E.J., Tian, Z., et al. (2014). Independent optical excitation of distinct neural populations. Nat. Meths. *11*, 338-351.
43. Lee, T., and Luo, L. (1999). Mosaic analysis with a repressible cell marker for studies of gene function in neuronal morphogenesis. Neuron *22*, 451-461.
44. Lee, H.-G., Rohila, S., and Han, K.-A. (2009). The octopamine receptor OAMB mediates ovulation via Ca^{2+}/calmodulin-dependent protein kinase II in the *Drosophila* oviduct epithelium. PLoS ONE *4*:e4716.
45. Li, W., Piëch, V., and Gilbert, C.D. (2004) Perceptual learning and top-down influences in primary visual cortex. Nature Neurosci. *7*, 651-657.
46. Lin, A.C., Bygrave, A.M., de Calignon, A., Lee, T., and Miesenböck, G. (2014). Sparse, decorrelated odor coding in the mushroom body enhances learned odor discrimination. Nat. Neurosci. *17*, 559–568.
47. Liu, C., Plaçais, P.Y., Yamagata, N., Pfeiffer, B., Aso. Y., Friedrich, A.B., Siwanowicz, I., Rubin, G.M., Preat, T., and Tanimoto, H. (2012). A subset of dopamine neurons signals reward for odour memory in *Drosophila*. Nature *488*, 512-517.
48. Maimon G., Straw A.D., and Dickinson M.H. (2010) Active flight increases the gain of visual motion processing in *Drosophila*. Nat Neurosci *13*, 393–399
49. Maqueira, B., Chatwin, H., and Evans, P.D. (2005). Identification and characterization of a novel family of *Drosophila* beta-adrenergic-like octopamine G-protein coupled receptors. J. Neurochem. *94*, 547–560.
50. Masuda-Nakagawa, L.M., Tanaka, N.K., and O'Kane, C.J. (2005). Stereotypic and random patterns of connectivity in the larval mushroom body calyx of *Drosophila*. Proc. Natl. Acad. Sci. USA. *102*, 19027–19032.
51. Masuda-Nakagawa, L.M., Gendre, N., O'Kane, C.J., and Stocker, R.F. (2009). Localized olfactory representation in mushroom bodies of *Drosophila* larvae. Proc. Natl. Acad. Sci. USA. *106*, 10314–10319.
52. Masuda-Nakagawa, L.M., Ito, K., Awasaki, T., and O'Kane, C.J. (2014). A single GABAergic neuron mediates feedback of odor-evoked signals in the mushroom body of larval *Drosophila*. Front. Neural Circuits *8*, 35.
53. Matsumoto, Y., Matsumoto, C.S., Wakuda, R., Ichihara., S, and Mizunami, M. (2015). Roles of octopamine and aversive memory acquisition stiudeies in olfactory conditioning of

maxillary palpi extension response in crickets. Front Behav. Neurosci. *9*, 230.

54. Menzel, R. (2012). The honeybee as a model for understanding the basis of cognition. Nature Revs. *13*, 758-768.
55. Morita, M., Susuki, J., Amino, H., Yoshiki, F., Moizumi, S., and Kudo, Y. (2006). Use of the exogenous Drosophila octopamine receptor gene to study Gq-coupled receptor-mediated responses in mammalian neurons. Neuroscience *137*, 545–553.
56. Nagarkar-Jaiswal, S., Lee, P., Campbell, M.E., Chen, K., Anguiano-zarate, S., Gutierrez, M.C., Busby, T., Lin, W., He, Y., Schulze, K.L., et al. (2015). A library of MiMICs allows tagging of genes and reversible spatial and temporal knockdown of proteins in *Drosophila*. eLife *4*, e05338.
57. Nai, Q., Dong, H-W., Hayar, A., Linster, Ch. and Ennis, M. (2009). Noradrenergic regulation of GABAergic inhibition of main olfactory bulb mitral cells varies as a function of concentration and receptor subtype. J. Neurophysiol. *101*, 2472-2484.
58. Nern, A., Pfeiffer, B.D., and Rubin, G.M. (2015). Optimized tools for multicolor stochastic labeling reveal diverse stereotyped cell arrangements in the fly visual system. Proc Natl. Acad. Sci. USA. *112*, E2967-E2076.
59. Nicolaï, L.J.J., Ramaekers, A., Ramaekers, T., Drozdzecki, A., Mauss, A.S., Yan, J., Landgraf, M., Annaert, W., and Hassan, B.A. (2010). Genetically encoded dendritic marker sheds light on neuronal connectivity in *Drosophila*. Proc. Natl. Acad. Sci. USA *107*, 20553-20558.
60. Pauls, D., Selcho, M., Gendre, N., Stocker, R.F., and Thum, A.S. (2010). *Drosophila* larvae establish appetitive olfactory memories via mushroom body neurons of embryonic origin. J. Neurosci. *30*, 10655-10666.
61. Pfeiffer, B.D., Ngo, T.-T.B., Hibbard, K.L., Murphy, C., Jenett, A., Truman, J.W., and Rubin, G.M. (2010). Refinement of tools for targeted gene expression in *Drosophila*. Genetics *186*, 735–755.
62. Pitman, J.L., Huetteroth, W., Burke, C.J., Krashes, M.J., Lai, S.-L., Lee, T., and Waddell, S. (2011). A pair of inhibitory neurons are required to sustain labile memory in the *Drosophila* mushroom body. Curr. Biol. *21*, 855-861.
63. Poo, C., and Isaacson, J.S. (2009). Odor representations in olfactory cortex: "sparse" coding, global inhibition, and oscillations. Neuron *62*, 850-861.
64. Reynolds, J.H., and Chelazzi, L. (2004). Attentional modulation of visual processing. Annu. Rev. Neurosci. *27*, 611-647.
65. Roeder, T., Seifert, M., Kähler, C., and Gewecke, M. (2003). Tyramine and octopamine: antagonistic modulators of behavior and metabolism. Arch. Insect. Biochem. Physiol. *54*,

1-13.

66. Sara, S.J. (2009). The locus coerulus and noradrenergic modulation of cognition. Nat. Revs. Neurosci. *10*, 211-223.
67. Sara, S.J. and Bouret, S (2012). Orienting and reorienting: the Locus Coeruleus mediates cognition through arousal. Neuron 76, 130-141.
68. Scherer, S., Stocker, R.F., and Gerber, B. (2003). Olfactory learning in individually assayed *Drosophila* larvae. Learning & Memory *10*, 217-225.
69. Schmidt, M.F. and Konishi, M. (1998). Gating of auditory responses in the vocal control system of awake songbirds. Nat. Neurosci. *1*, 513-518.
70. Schroll, C., Riemensperger, T., Bucher, D., Ehmer, J. Völler, T., Erbguth, K., Gerber, B., Hendel, T., Nagel, G., Buchner, E., and Fiala, A. (2006). Light-induced activation of distinct modulatory neurons triggers appetitive or aversive learning in *Drosophila* larvae. Curr. Biol. *16*, 1741-1747.
71. Schröter, U., Malun, D., and Menzel, R. (2007). Innervation pattern of suboesophageal ventral unpaired median neurones in the honeybee brain. Cell Tissue Res. *327*, 647-667.
72. Schwaerzel, M., Monastirioti, M., Scholz, H., Friggi-Grelin, F., Birman, S., and Heisenberg, M. (2003). Dopamine and octopamine differentiate between aversive and appetitive olfactory memories in *Drosophila*. J Neurosci. *23*, 10495-10502.
73. Selcho, M., Pauls, D., Huser, A., Stocker, R.F., and Thum, A.S. (2014). Characterization of the octopaminergic and tyraminergic neurons in the central brain of *Drosophila* larvae. J. Comp. Neurol. *522*, 3485–3500.
74. Selcho, M., Millán, C., Palacios-Muñoz, Ruf, F., Ubillo, L., Chen, J., Bergmann, G., Ito, C., Silva, V., Wegener, C., and Ewer, J. (2017). Central and peripheral clocks are coupled by a neuropeptide pathway in *Drosophila*. Nat. Comms. *8*, 15563.
75. Stettler, D.D., and Axel R. (2009). Representations of odor in the Piriform Cortex. Neuron 63, 854-864.
76. Stevenson, P.A., Dyakonova, V., Rillich, J., and Schildberger, K. (2005). Octopamine and experience-dependent modulation of aggression in crickets. J. Neurosci. *25*, 1431-1441.
77. Shearin, H.K., Dvarishkis, A.R., Kozeluh, C.D., and Stowers, R.S. (2013). Expansion of the Gateway Multisite Recombination Cloning Toolkit. PLoS ONE *8*, e77724.
78. Sinakevitch, I., Mustard, J.A., and Smith, B.H. (2011). Distribution of the octopamine receptor AmOA1 in the honey bee brain. PLoS One *6*, e14536.
79. Slater, G., Levy, P., Chan, K.L.A., and Larsen, C. (2015). A Central Neural Pathway Controlling Odor Tracking in *Drosophila*. J. Neurosci. *35*, 1831–1848.
80. Sombati, S., and Hoyle, G. (1984). Central nervous sensitization and dishabituation of

reflex action in an insect by the neuromodulator octopamine. J. Neurobiol. *15*, 455-480.

81. Sonnhammer, E.L., von Heijne, G., and Krogh, A. (1998). A hidden Markov model for predicting transmembrane helices in protein sequences. Proc. ISMB *6*, 175–182.
82. Stern, M. (2009). The PM1 neurons, movement-sensitive centrifugal visual brain neurons in the locust: anatomy, physiology and modulation by identified octopamnergic neurons. J. Comp. Physiol. A Neuroethol. Sens. Neural Behav. Physiol. *195*, 123-137.
83. Stevenson, P.A., Dyakonova, V., Rillich, J., and Schildberger, K. (2005). Octopamine and experience-dependent modulation of aggression in crickets. J. Neurosci. *25*, 1431-1441.
84. Stokes, C.C.A., and Isaacson, J.S. (2010). From dendrite to soma: dynamic routing of inhibition by complementary interneuron microcircuits in olfactory cortex. Neuron *67*, 452-465.
85. Stopfer, M., Bhagavan, S. Smith, B.H., and Laurent, G. (1997). Impaired odor discrimination on desynchronization of odor-encoding neural assemblies. Nature *390*, 70-74.
86. Strother, J. A., Wu, S.-T., Rogers, E. M., Eliason, J. L. M., Wong, A. M., Nern, A., and Reiser, M. B. (2018). Behavioral state modulates the ON visual motion pathway of *Drosophila*. Proc. Natl. Acad. Sci. USA *115*, E102-E111.
87. Suver, M.P., Mamiya, A., and Dickinson, M.H. (2012). Octopamine neurons mediate flight-induced modulation of visual processing in *Drosophila*. Curr. Biol. *22*, 2294-2302.
88. Szyszka, P., Galkin, A., and Menzil, R. (2008). Associative and non-associative plasticity in Kenyon cells of the honeybee mushroom body. Front. Syst. Neurosci. 2, 3.
89. Tanaka, N.K., Awasaki, T., Shimada, T., and Ito, K. (2004). Integration of Chemosensory Pathways in the *Drosophila* Second-Order Olfactory Centers. Curr. Biol. *14*, 449–457.
90. Treue, S., and Martinez Trujillo, J.C. (1999). Feature-based attention influences motion processing gain in macaque visual cortex. Nature *399*, 575-579.
91. Venken, K.J.T., Schulze, K.L., Haelterman, N. a, Pan, H., He, Y., Evans-Holm, M., Carlson, J.W., Levis, R.W., Spradling, A.C., Hoskins, R. a, et al. (2011). MiMIC: a highly versatile transposon insertion resource for engineering *Drosophila melanogaster* genes. Nat. Methods *8*, 737–743.
92. Wilson, D.A., and Sullivan, R.M. (2011). Cortical processing of odor objects. Neuron *72*, 506-519.
93. Zars, T., Fischer, M., Schulz, R., and Heisenberg, M. (2000) Localization of a short-term memory in *Drosophila*. Science *288*, 672-675.

.

Figure Legends

Figure 1. MutiColor FlpOut of *Tdc2-GAL4*-expressing neurons labels two calyx-innervating neurons. Single cell clones in larval progeny of *Tdc2-GAL4* crossed to *pBPhsFlp2::PEST(attP3); HA_V5_FLAG_OLLAS,* were generated by heat shock induction of FLP. **A.** 3D stereo projection of a neuron labeled in magenta (V5 tag) and another labeled in green (HA tag), both ramifying throughout the calyx. Arrowheads show the axons of the two neurons. Scale bar, 10 µm. **B**. Cell bodies in the SEZ of the same larva. In the mandibular (top) neuromere, two cell bodies labeled in magenta can be identified labeled by antibody to V5 (arrowheads). One of these is the sVUM1md neuron. In the maxillary (bottom) neuromere, a single cell body is only green, identified by anti-HA (arrowhead). Scale bar, 15 µm.

Figure 2. Polarity of calyx innervation by *Tdc2-GAL4*-expressing neurons. A. 3D stereo projection of a 3rd instar calyx expressing nSyb::GFP and CD4::Tom using *Tdc2-GAL4*. Two axonal tracts (arrowheads) enter the calyx and ramify throughout it (CD4::tdTom), while processes show nSyb::GFP in boutons (green). Note boutons at the borders of glomeruli (e.g. arrow) and core of the calyx (e.g. asterisk). **B.** Confocal section of a larval calyx expressing DenMark::mCherry and Syt::GFP using *Tdc2-GAL4*. **C.** Confocal section of a larval brain expressing DenMark::mCherry and Syt::GFP using *Tdc2-GAL4*. The primary processes of *Tdc2-GAL4*-expressing neurons in md (top arrowhead) and mx (bottom arrowhead) neuromeres are shown. **A**, **B**: Anterior is to the bottom, medial to the right. Right brain orientation is shown. Scale bars, 10 µm. **C**: Ventral view, anterior is to top. Scale bar, 50 µm.

Figure 3. GRASP shows calyx contacts of sVUM1 termini with PNs, larval APL, and *odd*-like neurons, and few KCs. A. GRASP signal between sVUM1 neurons (expressing *Tdc2-LexA*) and other calyx neurons expressing the *GAL4* lines shown, driving expression of GRASP constructs *UAS-CD4::spGFP1-10* and *LexAop-CD4::spGFP11*, is detected as native GFP fluorescence in confocal sections. Scale bar, 10 µm.

B-E. GRASP signal between sVUM1 neurons and other calyx neurons, from GRASP constructs driven by *Tdc2-LexA* and the *GAL4* lines shown, detected by anti-GFP. Examples of GRASP signal are highlighted with arrowheads; areas inside broken square are shown at higher zoom. sVUM1 termini are labeled using anti-OA, calyx glomeruli using anti-Dlg. Scale bars in main panels 10 µm, in insets 1 µm, here and throughout figure.

B. GRASP signal between sVUM1 termini and PNs, localized mainly around glomeruli. OA signals without GRASP are localized to the calyx core. Examples of GRASP signal are

highlighted with arrowheads. GRASP signal overlaps partially with sVUM1 termini labelled with OA (inset). Areas inside broken lines, here and subsequently, are shown at higher zoom.

C-E. GRASP signals between sVUM1 termini and KCs (**C**), Odd neurons (**D**), or the APL neuron (**E**). **E.** GRASP signals between sVUM1 and APL neurons are localized around glomeruli, or in the core of the calyx. Upper panels show extent of GRASP overlap with OA-containing sVUM1 terminals; Lower panels show some GRASP signals overlapping partially with large GABA boutons.

F. Confocal sections of a 3rd instar larval calyx expressing *mCD8::GFP* using *Tdc2-Gal4* and labeled with anti-GABA and anti-Dlg. Top is dorsal section of calyx, bottom is a ventral section of the same calyx. Arrowheads indicate GABA boutons apposed to or overlapping with *Tdc2* neuron terminals. Arrows indicate the two axonal tracts of *Tdc2* neurons innervating the calyx.

Figure 4. Single cell GRASP of sVUM1 neurons in the calyx. A. Identification of sVUM1 neurons based on SEZ anatomical landmarks. Larval brains carrying *Tdc2-LexA*, *GMR34A11-GAL4*, *LexAop-FLP*, *tub>GAL80>* and *UAS-Chrimson::Venus*, showing Venus expression in a subset of the cells expressing both *Tdc2-LexA* and *GMR34A11-GAL4*. sVUM1md neurons (Md) are in a small anterior medial Dlg-negative gap, with characteristic bilaterally symmetrical gaps (asterisks) nearby. sVUM1mx neurons (Mx) are localized in a large medial gap (arrowhead) that lies just anterior to a commissural DLG pathway (arrowheads). sVUMlb neurons (Lb) are localized posteriorly to this commissural pathway. Scale bar 24 μm.

B-D. Single-cell GRASP was induced between sVUM1 neurons expressing *Tdc2-LexA*, and potential calyx partner neurons that expressed different *GAL4* lines. sVUM1 neurons were individually labeled by heat-shock-induced FlipOut of larvae carrying *P{hsFLP}12, Tdc2-LexA, GAL4*, *LexAOp2-IVS>stop>spGFP11::CD4::HA-T2A-Brp::mCherry (attP2), UAS-spGFP1-10::CD4, UAS- HRP::CD2*.

B. Single cell clone generation showing expression of Brp::mCherry in subsets of *Tdc2-LexA*-expressing neurons; each row shows a separate clone. Left image pairs are stereo views of reconstructions showing the entire trajectory of labelled neurons; right images are single confocal sections through the SEZ of the same larvae, showing the primary process of each labelled sVUM1 (arrows) and the anatomical landmarks shown in **A**. First row, sVUMmd1 and sVUMmx1. Second row, sVUMmd1. Third row, sVUMmx1. Scale bar is 45 μm in 3D images (Left), 30 μm in SEZ sections (Right).

C-D. Single-cell GRASP between sVUM1 neurons expressing *Tdc2-LexA*, and (**C**) Odd neurons expressing *OK263-GAL4*, or (**D**) larval APL expressing *NP2631-GAL4*. Left panels: larval calyx labelled with anti-DsRed to visualize Brp::mCherry (enriched at presynaptic sites

but not confined to them), anti-Dlg to label neuropile, and anti-GFP to visualize GRASP signals. Arrows indicate GRASP signals. Scale bar: 10 µm. Right panel: region of same brain labelled with anti-Dlg to visualize neuropile, and anti-DsRed to visualize the VUM neurons. Top rows show sVUMmd1 (Md), bottom rows show sVUMmx1 (Mx). Arrows indicate the primary process of each sVUM1 neuron.

Figure 5. Oamb-GFP localization in PN presynaptic termini. **A.** Calyces of a larva carrying *Oamb::EFGP*, *NP225-GAL4* and *UAS-RFP* labelled with antibodies to GFP, DsRed and Dlg. Oamb::EGFP localizes to PN terminals in all glomeruli labeled by *NP225-GAL4*, and to a few additional glomeruli innervated by PNs, not labeled by *NP225-GAL4* (arrowheads). A few glomeruli show neither *NP225-GAL4* nor Oamb::EFGP expression (asterisks). **B.** Oamb::EGFP does not overlap with APL termini labeled by anti-GABA (top row) or with APL projections labeled using *NP0732-GAL4* (bottom row). **C.** Oamb::EGFP does not overlap substantially with Odd neuron dendrites labeled by *OK263-GAL4*. Scale bar, 10 µm.

Figure 6. Activation of Tdc2-expressing neurons potentiates presynaptic activity of calyx PN terminals. A. Examples of odor-evoked jRCaMP1b responses in PN terminals, in a control calyx (*WT*, carrying *NP225-GAL4* to drive *jRCaMP1b*, and *LexAop-ChR2(XXL)* but no *LexA* driver) and a similar calyx (*Tdc2*) that also carried *Tdc2-LexA* to drive ChR2(XXL) expression in OA neurons. For each genotype, the top row shows the calyx at rest (left image) and stimulated by an odor pulse (right image); the bottom row shows a response in the same calyx, 0.5 s after a 2-s blue light pulse to activate ChR2(XXL). Magnified insets show false color of odor-evoked activity (∆F/F), integrated over the 6 seconds from the end of the odor pulse to the end of acquisition. Grayscale panes 40x40 µm; false color panels, 20x20 µm **B.** Graphs show averaged recordings from larvae (n=24) expressing *UAS-jRCaMP1b* in PNs under control of *NP225-GAL4*, and carrying *LexAop-Chr2(XXL)* either without (*WT*, left graph) or with *Tdc2-LexA* (*Tdc2*, right graph). Black lines show the PN terminal response (∆F/F) to a 2-second odor pulse (black bars). Blue lines show subsequent responses from the same brains, after activation of ChR2(XXL) by a blue light pulse (blue bar) before the odor pulse; ∆F/F response to light alone without odor is subtracted from each response, and a bleach correction factor is applied to each individual response, calculated from the averaged response to Light+Odor in the WT control larvae. Graphs show mean + SEM. **C.** Comparisons of integrated ∆F/F odor-evoked responses from calyces used in (**B**), without ("Odor") or following optogenetic stimulation ("Light+Odor"). Each datapoint shows ∆F/F integrated over 6 seconds, from the end of the odor stimulus to the end of acquisition. Violin plots reflect the distribution

of datapoints. The left graph shows the control line lacking *Tdc2-LexA* to drive ChR2(XXL) expression; the right graph shows the line containing *Tdc2-LexA*. Comparisons are performed using a Wilcoxon matched-pairs signed rank test.

Figure 7. Behavioral discrimination assay and optogenetics. Larvae are conditioned for three cycles of: a container with one odor (in this case ethyl acetate, EA) and a container lacking odor (C) on a agar sucrose plate (red), followed by a container with a different odor (in this case pentyl acetate, PA) and a container lacking odor, on an agar plate (light gray). Larvae are then tested by being placed on an oblong area in the middle of an agar plate, with a choice of EA or PA, and a black background to provide contrast for counting larvae. A different group of larvae are conditioned and tested with reciprocal odor pairing. Control experiments (top row) are carried out in dim blue light. Optogenetic activation of CsChrimson is accomplished by amber light during the conditioning phases.

Figure 8. Activation of a small subset of OA neurons including the sVUM1 neurons disrupts odor discrimination but not learning. A. A pair of stereo images showing CsChrimson::mVenus expressed in a small subset of OA neurons, using the genotype shown in Fig. 4A. The mandibular, maxillary and labial (Md, Mx, Lb) clusters are shown, which include the sVUMmd1 and sVUMmx1 neurons. Scale bar, 40 μm. **B.** Activation of the neurons labelled in A by CsChrimson occurs in the presence of retinal and amber light, and abolishes odor choice learning using similar odor pairs, compared to controls exposed to blue light, lacking retinal, or tested with dissimilar odor pairs. No effect of CsChrimson activation is seen on learning using dissimilar odor pairs. Planned statistical comparisons shown are t-tests (***, $P < 0.0001$, NS, $P > 0.6$). An ANOVA test across all data from two experimenters showed no significant effect of experimenter either alone, or as interactions with other factors ($P>0.2$). ANOVA tests also showed no significant effect of odor alone ($P>0.03$, not significant with multiple testing), retinal alone ($P>0.4$), or light alone ($P>0.2$), when comparisons that would have included the retinal, amber, similar combination with the strong effect were excluded.

Table 1. *Drosophila* stocks used.

Genotype	Source	Reference	RRID	Use	Figure
NP2631-GAL4 (II)	T Awasaki, K Ito	Masuda-Nakagawa et al., 2014	DGGR_104266	APL neuron	3A,E, 4D
NP0732-GAL4 (I)	T Awasaki, K Ito	Masuda-Nakagawa et al., 2014	DGGR_112307	APL neuron	5B
NP225-GAL4 (II)	T Awasaki, K Ito	Masuda-Nakagawa et al. 2005	DGGR_112095	PN	3A,B, 5A, 6
OK263-GAL4 (II)	COK, LMN	This work		*Odd* neurons	3A,D, 4C, 5C
MB247-GAL4 (III)	BDSC 50742	Zars et al. 2000	BDSC_50742	KCs	3A,C
GMR34A11-GAL4 (III)	BDSC 49767	Jenett et al., 2012	BDSC_49767	sVUM1 neuron	4A, 8
Tdc2-GAL4 (II)	BDSC 9313	Cole et al., 2005	BDSC_9313	OA neuron	1, 2, 3F
Tdc2-LexA (II)	S Certel, S Waddell	Burke et al., 2012		OA neuron	3, 4
Tdc2-LexA (III)	S Certel, S Waddell	Burke et al., 2012		OA neuron	3, 6
MB247-LexA (III)	T Lee	Pitman et al., 2011		KC	
GMR34A11-LexA (II)	BDSC 52755	Jenett et al, 2012	BDSC_52755	sVUM1	
UAS-mCD8::GFP (III)	BDSC 5130	Lee and Luo, 1999	BDSC_5130	mCD8::GFP reporter	3F, 5B,C
10XUAS-IVS-mCD8::RFP (attP40) (II)	BDSC 32219	Pfeiffer et al., 2010	BDSC_32219	mCD8::RFP reporter	5
13XLexAOp-mCD8::GFP (III)	BDSC 32203	Pfeiffer et al., 2010	BDSC_32203	mCD8::GFP reporter	
UAS-CD4::tdTomato (II)	BDSC 35841	Han et al., 2011	BDSC_35841	Neuronal polarity	2A
UAS-nSyb::GFP	M Ramaswami	Estes et al., 2000		Neuronal polarity	2A
UAS-Syt::GFP UAS-DenMark::mCherry (III)	BDSC 33065	Nicolaï et al., 2010	BDSC_33065	Neuronal polarity	2B,C
10XUAS-IVS-mCD8::RFP, 13XlexAOp2-mCD8::GFP (X)	BDSC 32229	Pfeiffer et al., 2010	BDSC_32229	Double Reporter	
UAS-CD4::spGFP1-10	K Scott	Gordon and Scott, 2009		GRASP	3
LexAop-CD4::spGFP11	K Scott	Gordon and Scott, 2009		GRASP	3
LexAOp2-IVS>stop>spGFP11::CD4::HA-T2A-Brp::mCherry (attP2), UAS-spGFP1-10::CD4, UAS- HRP::CD2	C-H Lee	Karuppudurai et al., 2014		Single cell GRASP	4B-D
P{hsFLP}12 y w; CyO/Sco	BDSC 1929		BDSC_1929	Single cell GRASP	4B-D
pBPhsFlp2::PEST(attP3); +; HA_V5_FLAG_OLLAS (III)	M Landgraf	Nern et al., 2015	BDSC_64086	Multicolor Flpout (MCFO-2)	1
nSyb-LexA (II)	M Landgraf	Shearin et al., 2013	BDSC_52247	Pan-neuronal LexA	
LexAop-ChR2-XXL (II)	C Wegener (955)	Selcho et al., 2017		ChR2-XXL	6
w; Pbac{w20XUAS-IVS-NES-jRCaMP1b-p10}VK00005 (III)*	BDSC 63793	Dana et al., 2016	BDSC_63793	jRCaMP1b Reporter	6
Tub84B(FRT-GAL80)1, w; Bl/CyO; TM2/TM6B	BDSC 38879		BDSC_38879	sVUM1 instersection	4A, 8
P{8xLexAop2-FLPL}attP40 (II)	B Pfeiffer, Janelia		BDSC_55820	sVUM1 instersection	4A, 8
UAS-Chrimson::mVenus (III)	BDSC 55136	Klapoetke et al., 2014	BDSC_55136	Effector/reporter for intersectional lines	4A, 8
y^1 w^*; +; Mi{MIC}Oamb^{MI12417}	BDSC 57940	Venken et al., 2011	BDSC_57940	Progenitor of *Oamb::EGFP*	

y^{1} *w***; +; Mi{PT-GFSTF.1}Oamb*$^{MI12417\text{-}GFSTF.1}$*/TM6C*	Fly Facility, Dept. of Genetics	This work		*Oamb::EGFP*	5
Mi{MIC}Octβ1R^{MI05807}	BDSC 42119	Venken et al., 2011	BDSC_42119	Progenitor of *Octβ1R::EGFP*	
Mi{MIC}Octβ2R^{MI13416}	BDSC 59133	Venken et al., 2011	BDSC_59133	Progenitor of *Octβ2R::EGFP*	
Mi{MIC}Octβ2R^{MI06217}	BDSC 43050	Venken et al., 2011	BDSC_59133	Progenitor of *Octβ3R::EGFP*	
Mi{PT-GFSTF.2}Octβ1R$^{MI05807\text{-}GFSTF.2}$	BDSC 60236	Venken et al., 2011	BDSC_60236	*Octβ1R::EGFP*	
Mi{PT-GFSTF.2}Octβ2R$^{MI13416\text{-}GFSTF.2}$	Fly Facility, Dept. of Genetics	This work		*Octβ2R::EGFP*	
Mi{PT-GFSTF.0}Octβ3R$^{MI06217\text{-}GFSTF.0}$	Fly Facility, Dept. of Genetics	This work		*Octβ3R::EGFP line, GFP intron phase 0*	
Mi{PT-GFSTF.1}Octβ3R$^{MI06217\text{-}GFSTF.1}$	BDSC 60245	Nagarkar-Jaiswal et al., 2015	BDSC_60245	*Octβ3R::EGFP line, GFP intron phase 1*	

Table 2. Primers

Primer	Sequence	Purpose
MiMIC-5R	CTTGAGATTAAGGTAGCTTACGC	Verifying Mi{MIC} insertion
MiMIC-3F	TGCAGGTCGACGAATTCAAC	Verifying Mi{MIC} insertion
MI12417-5F	CCACAATCAACGTCCTGCTC	Verifying Mi{MIC} insertion
MI12417-3R	GATTATCGCCACCACAGAGTC	Verifying Mi{MIC} insertion
MI05807-5F	TCCTTTCATTCCCGAGCACC	Verifying Mi{MIC} insertion
MI05807-3R	CTCGTTAACAATCGCTCGCC	Verifying Mi{MIC} insertion
MI13416-5F1	CGGAGTCACTGAGTAATGGCG	Verifying Mi{MIC} insertion
MI13416-5F2	ATGGCGAGTGGTATGAGCAG	Verifying Mi{MIC} insertion
MI13416-5F3	GTGCTCTAGATGGCGAGTGG	Verifying Mi{MIC} insertion
MI13416-5F4	ACCGAGGCTCATTAACACAG	Verifying Mi{MIC} insertion
MI13416-5F5	GAGGCTCATTAACACAGCGC	Verifying Mi{MIC} insertion
MI13416-3R	GCTGCCTCATTGAACTCCAG	Verifying Mi{MIC} insertion
MI06217-5F	GCAGGAGAACAGCGACAGTC	Verifying Mi{MIC} insertion
MI06217-3R	CCTGTCTCTGGAAGTAGGTCG	Verifying Mi{MIC} insertion
Orientation-MiL-F (OriF)	GCGTAAGCTACCTTAATCTCAAGAAGAG	Verifying GFP swap orientation
Orientation-MiL-R (OriR)	CGCGGCGTAATGTGATTTACTATCATAC	Verifying GFP swap orientation
EGFPdo-Seq-F (EGFP-F)	GGATGACGGCACCTACAAGAC	Verifying GFP swap orientation
EGFPdo-Seq-R (EGFP-R)	GTGGCTGTTGAAGTTGTACTC	Verifying GFP swap orientation

Table 3. Antibodies

Antibody	**Host**	**Source**	RRID	**Dilution**	**Experiment or Figures**
Anti-GFP	Rat, monoclonal	Nacalai 440426 (Clone GF090R)	AB_2314545	1:1000	GRASP (3B,C,D,E) UAS-CD8::GFP
Anti-GFP	Chicken, polyclonal	Abcam, Ab13970	AB_300798	1:1000/ 1:2000	Oamb::EGFP (5)
Anti-GFP	Rabbit, polyclonal	Invitrogen, A11122	AB_221569	1:1000/ 1:2000	
Anti-GFP	Rabbit, polyclonal	Abcam, Ab290	AB_303395	1:800	
Anti-DsRed	Rabbit, polyclonal	Clontech, 632496	AB_10013483	1:1000	UAS-tdTom (2A), UAS-DenMark (2B,C) Brp::mCherry (4B,C,D) UAS-RFP (5),
Anti-GABA	Rabbit, polyclonal	Sigma, A2052	AB_477652	1:1000	Figs. 3E,F, 5B
Anti-OA	Rabbit, polyclonal	MoBiTec, 1003GE	AB_2314999	1:1000	Figs 3B-E
Anti-Dlg	Mouse, monoclonal	DSHB, 4F3	AB_528203	1:200	Figs. 2-5
Anti-FLAG	Mouse, monoclonal	Sigma, F1804	AB_262044	1:4000	MCFO
Anti-HA	Rat, monoclonal	Roche, 3F10	AB_2314622)	1:1000	MCFO (1A,B)
Anti-V5	Chicken, polyclonal	Abcam Ab1993	AB_302743	1:1000	MCFO (1A,B)
Secondary Antibody	**Host**	**Source**		**Dilution**	
Anti-Rat Alexa 488	Goat, polyclonal	Invitrogen, A11006	AB_2534074	1:200	
Anti-Rat Alexa 594	Goat, polyclonal	Invitrogen, A11007	AB_10561522	1:200	
Anti-Chicken Alexa 488	Goat, polyclonal	Invitrogen, A11039	AB_142924	1:200	
Anti-Rabbit Alexa 488	Goat, polyclonal	Invitrogen, A11034	AB_2576217	1:200	
Anti-Rabbit Alexa 568	Goat, polyclonal	Invitrogen, A11036	AB_10563566	1:200	
Anti-Mouse Alexa 647	Goat, polyclonal	Invitrogen, A21236	AB_141725	1:200	
Anti-Rabbit Alexa 647	Goat, polyclonal	Invitrogen, A21245	AB_2535813	1:200	
Anti-Chicken Alexa 568	Goat, polyclonal	Invitrogen, A11041	AB_2534098	1:200	

Table 4. Other reagents

Reagent	**Source**	**Experiment or Figures**
Paraffin oil	Sigma-Aldrich, 76235	Behavior
Pentyl Acetate	Sigma-Aldrich, 109584	Behavior
Ethyl Acetate	Sigma-Aldrich, 319902	Behavior
Ethanol	Sigma-Aldrich, 32221	Behavior
all-trans-retinal (ATR)	Sigma-Aldrich, R2500	Behavior
D-(-)-Fructose	Sigma-Aldrich, 47740	Behavior
Agarose	Sigma-Aldrich, A9539	Behavior

Supplementary Figure Legends

Supplementary Fig. 1. PCR verification of *MI12417(Oamb)* insertion in the *Oamb* gene. **(A)** Primers designed against 5' (*MI12417-5F/MiMIC-5R*) and 3' (*MiMIC-3F/MI12417-3R*) *MiMIC* insertion flanking ends were used to validate the *MI12417* insertion in the *Oamb* gene. **(B)** PCR results for *MI12417* MiMIC insertion. PCR products were detected for *MI12417* 5' and 3' flanking ends using *MI12417* DNA template, but not for negative control template (denoted as +). A PCR product was detected using primers against the *Oamb* genomic flanking sequences (*MI12417-5F/MI12417-3R)* for the negative control lacking *MI12417* insertion, as well as for *MI12417* due to heterozygosity of the insertion. Abbreviations: MiL/MiR, *MiMIC* insertion ends Left/Right. SA, Splice Acceptor Site.

A

B

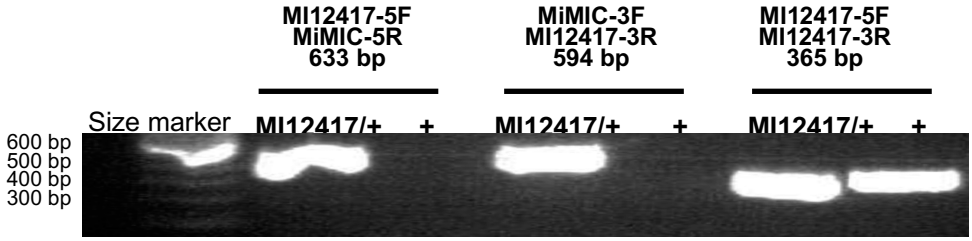

Supplementary Fig. 2. Alignment of *MI12417* 5' flanking PCR products to MiMIC and Oamb genomic sequences. (A) Sequenced 5' *MI12417* PCR product. Alignment to MiMIC sequences is indicated in yellow, alignment to *Oamb* in grey. Overlapping alignment at the MiMIC insertion site (TA) indicated in red. **(B-C)** Alignment of *MI12417* 5' PCR products to MiMIC **(B)** and *Drosophila melanogaster* **(C)** sequences using Nucleotide BLAST (Altschul et al., 1990).

A. Sequence of *MI12417* 5' flanking end

```
NTCTTTATTCGCATAATATAAATCACATGGCTCAAAGAAGAAGTCACGCATCATAATTAG
CATTATATTCCAAGTTGGGCAAAAACAAGAAATCGATAAACGCTGAGGAAGCACATCAAA
CAAATCGGCTTAGATAAAATTGAGGTTGGGATTAAATAGGAGCGGGATTCCAGCCAGAAA
ATGGCAGACATGAAAGCGAGCCATCGGCTAAAACGAAATAAAATATACGAGCCCCAACCA
CTATTAATTCGAACAGCATGTTTTTTTGCAGTGCGCAATGTTTAACACACTATATTATCA
ATACTACTAAAGATAACACATACCAATGCATTTCGTCTCAAAGAGAATTTTATTCTCTTC
ACGACGAAAAAAAAAGTTTTGCTCTATTTCCAACAACAACAAAAATATGAGTAATTTATT
CAAACGGTTTGCTTAAGAGATAAGAAAAAAGTGACCACTATTAATTCGAACGCGGCGTAA
GCTACTAAATCTCTCANGAA
```

B. *MI12417* 5' flanking end alignment with *Oamb*

```
>AE014297.3 Drosophila melanogaster chromosome 3R      Length=32079331
Features in this part of subject sequence:
   octopamine receptor in mushroom bodies, isoform D
   octopamine receptor in mushroom bodies, isoform G

Strand=Plus/Minus
Query  71        CAAGTTGGGCAAAAACAAGAAATCGATAAACGCTGAGGAAGCACATCAAACAAATCGGCT  130
                 ||||||||||||||||||||||||||||||||||||||||||||||||||||||||||||
Sbjct  20697214  CAAGTTGGGCAAAAACAAGAAATCGATAAACGCTGAGGAAGCACATCAAACAAATCGGCT  20697155

Query  131       TAGATAAAATTGAGGTTGGGATTAAATAGGAGCGGGATTCCAGCCAGAAAATGGCAGACA  190
                 ||||||||||||||||||||||||||||||||||||||||||||||||||||||||||||
Sbjct  20697154  TAGATAAAATTGAGGTTGGGATTAAATAGGAGCGGGATTCCAGCCAGAAAATGGCAGACA  20697095

Query  191       TGAAAGCGAGCCATCGGCTAAAACGAAATAAAATATA  227
                 |||||||||||||||||||||||||||||||||||||
Sbjct  20697094  TGAAAGCGAGCCATCGGCTAAAACGAAATAAAATATA  20697058
```

C. *MI12417* 5' flanking end alignment with MiMIC sequences

```
>GU370067.1 Synthetic construct MIMIC transposable element, complete sequence   Length=7267

Strand=Plus/Plus
Query  226  TACGAGCCCCAACCACTATTAATTCGAACAGCATGttttttttGCAGTGCGCAATGTTTAA  285
            ||||||||||||||||||||||||||||||||||||||||||||||||||||||||||||
Sbjct  102  TACGAGCCCCAACCACTATTAATTCGAACAGCATGTTTTTTTGCAGTGCGCAATGTTTAA  161

Query  286  CACACTATATTATCAATACTACTAAAGATAACACATACCAATGCATTTCGTCTCAAAGAG  345
            ||||||||||||||||||||||||||||||||||||||||||||||||||||||||||||
Sbjct  162  CACACTATATTATCAATACTACTAAAGATAACACATACCAATGCATTTCGTCTCAAAGAG  221

Query  346  AATTTTATTCTCTTCACGACGaaaaaaaaaGTTTTGCTCTATTTCCAACAACAACAAAAA  405
            ||||||||||||||||||||||||||||||||||||||||||||||||||||||||||||
Sbjct  222  AATTTTATTCTCTTCACGACGAAAAAAAAAGTTTTGCTCTATTTCCAACAACAACAAAAA  281

Query  406  TATGAGTAATTTATTCAAACGGTTTGCTTAAGAGATAAGAAAAAAGTGACCACTATTAAT  465
            ||||||||||||||||||||||||||||||||||||||||||||||||||||||||||||
Sbjct  282  TATGAGTAATTTATTCAAACGGTTTGCTTAAGAGATAAGAAAAAAGTGACCACTATTAAT  341
```

Supplementary Fig. 3. Alignment of 3' flanking PCR products from *MI12417* to MiMIC and Oamb genomic sequences (A) Sequenced 3' *MI12417* PCR product. Alignment to MiMIC sequences are indicated in yellow, alignment to *Oamb* sequences in grey. Overlapping alignment at the MiMIC insertion site (TA) indicated in red. **(B-C)** Alignment of *MI12417* 3' PCR products to MiMIC **(B)** and *Drosophila melanogaster* **(C)** sequences using Nucleotide BLAST (Altschul et al., 1990).

A. Sequence of *MI12417* 3' flanking end

```
GCGGGAGTCGCGACTACGCCCCCACTGAGAGACTCAAAGGTTTACCCCAGTTGGGGCACT
ACTCCCGAAAACCGCTTCTGACCTGGGCCGCGGGGGAAATTAATTAAATTATTGTTTTAA
GTATGATAGTAAATCACATTACGCCGCGTTCGAATTAATAGTGGTCACTTTTTTCTTATC
TCTTAAGCAAACCGTTTGAATAAATTACTCATATTTTTGTTGTTGTTGGAAATAGAGCAA
AACTTTTTTTTTCGTCGTGAAGAGAATAAAATTCTCTTTGAGACGAAATGCATTGGTATG
TGTTATCTTTAGTAGTATTGATAATATAGTGTGTTAAACATTGCGCACTGCAAAAAAAAC
ATGCTGTTCGAATTAATAGTGGTTGGGGCTCGTAATATGTCTTCCCTGTTAGCATGTTCT
GTTTGCAATTTTCTATTTTCTTAGGTTTTTGTCGTTTCAGGCCTCACTGGTCCCCAAAGA
CTCTGTGGGGCCGGATAATCGGCTTTGTTCTGACAGCCGTTTTTTTGCTGGGCTGAATGT
TTAACACACTGGACCATCAGTTTGACTCAGGACTCACGGACCAGTGGCTCCTCCTCTCAA
AGAGAGTTTTATTCTCCTCGCCACAGCAAGGAAGGCCCTGCACGATGTCGAACAGGACCC
CGTGTGGCTCATCTCTTGCTTCTGTGGGAGGCAAGTCTAACCCAGTGTGACCTCCATGAA
GTCGAGAACAAGTAACTCAATCTCCCATCCCACCCTTATGCTGCGCCAGACCCGTGAGGA
GCCCACCTCCGGTGGACAC
```

B. *MI12417* 3' flanking end alignment with MiMIC sequences

```
>AE014297.3 Drosophila melanogaster chromosome 3R      Length=32079331
Features in this part of subject sequence:
   octopamine receptor in mushroom bodies, isoform D
   octopamine receptor in mushroom bodies, isoform G

>GU370067.1 Synthetic construct MIMIC transposable element, complete sequence   Length=7267
Strand=Plus/Plus
Query  252   tCGTCGTGAAGAGAATAAAATTCTCTTTGAGACGAAATGCATTGGTATGTGTTATCTTTA  311
              ||||||||||||||||||||||||||||||||||||||||||||||||||||||||||||
Sbjct  7062  TCGTCGTGAAGAGAATAAAATTCTCTTTGAGACGAAATGCATTGGTATGTGTTATCTTTA  7121

Query  312   GTAGTATTGATAATATAGTGTGTTAAACATTGCGCACTGCaaaaaaaaCATGCTGTTCGA  371
              ||||||||||||||||||||||||||||||||||||||||||||||||||||||||||||
Sbjct  7122  GTAGTATTGATAATATAGTGTGTTAAACATTGCGCACTGCAAAAAAAACATGCTGTTCGA  7181

Query  372   ATTAATAGTGGTTGGGGCTCGTA  394
              |||||||||||||||||||||||
Sbjct  7182  ATTAATAGTGGTTGGGGCTCGTA  7204
```

C. *MI12417* 3' flanking end alignment with *Oamb* sequences

```
>AE014297.3 Drosophila melanogaster chromosome 3R     Length=32079331
Features in this part of subject sequence:
   octopamine receptor in mushroom bodies, isoform D
   octopamine receptor in mushroom bodies, isoform G

Strand=Plus/Minus
Query  393       TAATATGTCTTCCCTGTTAGCATGTTCTGTTTGCAATTTTCTATTTTCTTAGGTTTTTGT  452
                  ||||||||||||||||||||||||||||||||||||||||||||||||||||||||||||
Sbjct  20697059  TAATATGTCTTCCCTGTTAGCATGTTCTGTTTGCAATTTTCTATTTTCTTAGGTTTTTGT  20697000

Query  453       CGTTTCAGGCCTCACTGGTCCCCAAAGACTCTGTGGGGCCGGATAATC  500
                  |||||||||||||||||||||||||||| |||||| | || ||||||
Sbjct  20696999  CGTTTCAGGCCTCACTGGTCCCCAAAGACGCTGTGGTGGCG-ATAATC  20696953
```

Supplementary Fig. 4. *MI12417* is inserted in coding intron 3 of *Oamb*. (A) Extract of TBLASTN query of Oamb-B against the *Drosophila* genome assembly, showing an intron at coordinates 20693849–20698333, inserted at amino-acid residue 338 of Oamb-B. **(B)**. Extract of BLASTN search of *Oamb-B* RNA, showing a splice site between nucleotides 2007 and 2008. **(C)** Alignment of Oamb-B protein and Oamb-B RNA sequences around the third intron, highlighting residue G338 and the AGGG splice site in yellow. **(D)** Map of *MI12417* insertion (3R:20,697,059) relative to *Oamb* gene and transcripts (Adapted from GBrowse, www.flybase.org).

A

```
Oamb-B:       284 PWKCELTNDRGYVLYSALGSFYIPMFVMLFFYWRIYRAAVRTTRAINQGFKTTKG 338
                  PWKCELTNDRGYVLYSALGSFYIPMFVMLFFYWRIYRAAVRTTRAINQGFKTTKG
Genome: 20698497 PWKCELTNDRGYVLYSALGSFYIPMFVMLFFYWRIYRAAVRTTRAINQGFKTTKG 20698333

Oamb-B:       338 GSPRESGNNRVDESQLILRIHRGRPCSTPQRTPLSVHSMSSTLSVNSNGGGGGAVASGLG 397
                  GSPRESGNNRVDESQLILRIHRGRPCSTPQRTPLSVHSMSSTLSVNSNGGGGGAVASGLG
Genome: 20693849 GSPRESGNNRVDESQLILRIHRGRPCSTPQRTPLSVHSMSSTLSVNSNGGGGGAVASGLG 20693670
```

B

```
Oamb-B:      1964 TGAGAACGACGAGAGCCATCAACCAGGGCTTCAAGACCACCAAG 2007
                  |||||||||||||||||||||||||||||||||||||||||||
Genome: 20698379 TGAGAACGACGAGAGCCATCAACCAGGGCTTCAAGACCACCAAG 20698332

Oamb-B:      2008 GGCAGTCCCCGCGAGTCGGGCAACAATCGAGTGGACGAGTCCCAGCTCATATTGCGCATT 2067
                  ||||||||||||||||||||||||||||||||||||||||||||||||||||||||||||
Genome: 20693849 GGCAGTCCCCGCGAGTCGGGCAACAATCGAGTGGACGAGTCCCAGCTCATATTGCGCATT 20693790
```

C

```
                                  Coding intron 3; 3R:20,697,059
                                  Exon 4>3R:20,693,848-20,692,947
    ATCAACCAGGGCTTCAAGACCACCAAGGGCAGTCCCCGCGAGTCGGGCAACAATCGAGTG
329 -I--N--Q--G--F--K--T--T--K--G--S--P--R--E--S--G--N--N--R--V-
```

D

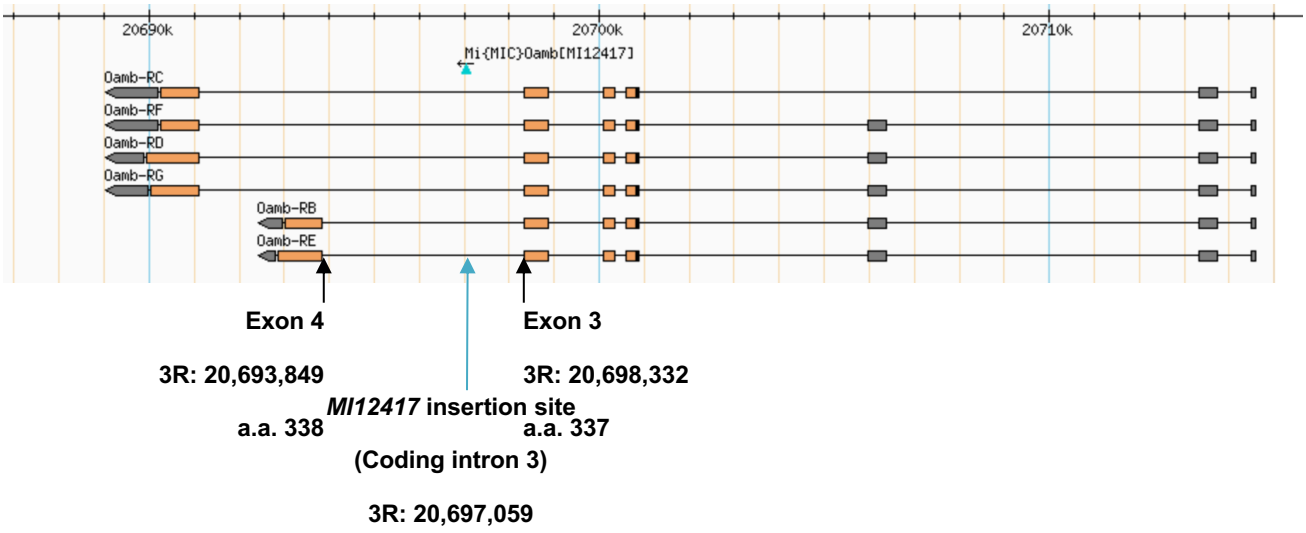

Supplemmentary Fig. 5. TMHMM predictions of transmembrane domains for Oamb-PB and PC isotypes. The third intracellular loop, where residue G338 is found, is highlighted in yellow.

A. Oamb-PB TMHMM Predictions

WEBSEQUENCE	TMHMM2.0	outside	1	21
WEBSEQUENCE	TMHMM2.0	TMhelix	22	44
WEBSEQUENCE	TMHMM2.0	inside	45	56
WEBSEQUENCE	TMHMM2.0	TMhelix	57	79
WEBSEQUENCE	TMHMM2.0	outside	80	93
WEBSEQUENCE	TMHMM2.0	TMhelix	94	116
WEBSEQUENCE	TMHMM2.0	inside	117	136
WEBSEQUENCE	TMHMM2.0	TMhelix	137	159
WEBSEQUENCE	TMHMM2.0	outside	160	293
WEBSEQUENCE	TMHMM2.0	TMhelix	294	316
WEBSEQUENCE	TMHMM2.0	inside	317	523
WEBSEQUENCE	TMHMM2.0	TMhelix	524	546
WEBSEQUENCE	TMHMM2.0	outside	547	555
WEBSEQUENCE	TMHMM2.0	TMhelix	556	578
WEBSEQUENCE	TMHMM2.0	inside	579	637

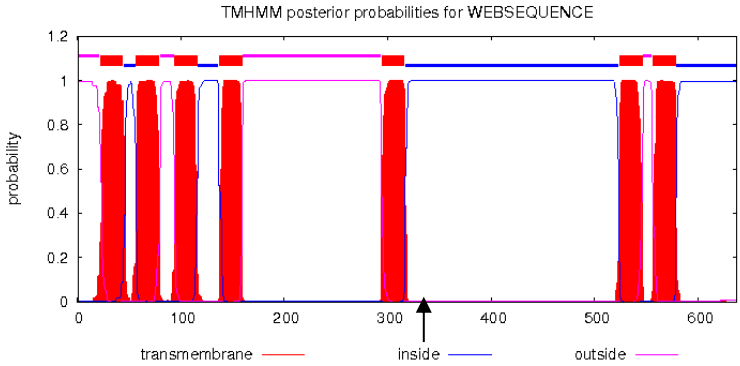

B. Oamb-PC TMHMM Predictions

WEBSEQUENCE	TMHMM2.0	outside	1	21
WEBSEQUENCE	TMHMM2.0	TMhelix	22	44
WEBSEQUENCE	TMHMM2.0	inside	45	56
WEBSEQUENCE	TMHMM2.0	TMhelix	57	79
WEBSEQUENCE	TMHMM2.0	outside	80	93
WEBSEQUENCE	TMHMM2.0	TMhelix	94	116
WEBSEQUENCE	TMHMM2.0	inside	117	136
WEBSEQUENCE	TMHMM2.0	TMhelix	137	159
WEBSEQUENCE	TMHMM2.0	outside	160	293
WEBSEQUENCE	TMHMM2.0	TMhelix	294	316
WEBSEQUENCE	TMHMM2.0	inside	317	520
WEBSEQUENCE	TMHMM2.0	TMhelix	521	543
WEBSEQUENCE	TMHMM2.0	outside	544	552
WEBSEQUENCE	TMHMM2.0	TMhelix	553	575
WEBSEQUENCE	TMHMM2.0	inside	576	645

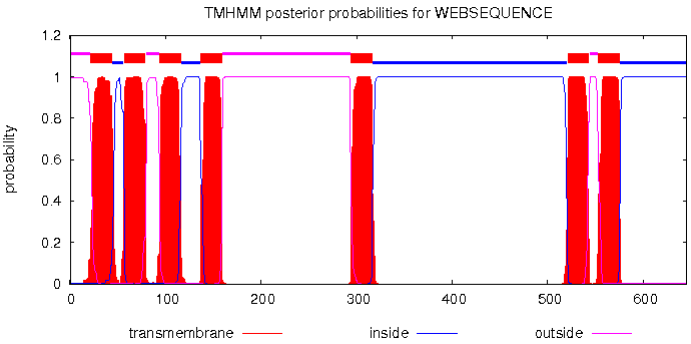

Supplementary Fig. 6. *MI12417* insertion location relative to *Oamb* cDNA and protein sequences. cDNA and protein sequences were taken from the ENSEMBL database (Aken et al., 2016; http://www.ensembl.org) for representative *Oamb* transcript protein isotype B. The beginning and range of each exon, obtained from the ENSEMBL database, is annotated in yellow. Transmembrane domains are indicated in green. MiMIC insertion location site, listed on the Gene Disruption Project database, is annotated in light blue. Abbreviations: TM, transmembrane domain; a.a., amino acid

```
3R:20,700,845
Exon 1>3R:20,700,845-20,700,594
    1  ATGAATGAAACAGAGTGCGAGGAT
    1  -M--N--E--T--E--C--E--D-
                                              TM I: a.a.22-44
   25 CTCATCAAATCTGTGAAATGGACGGAACCAGCCAATCTGATCTCCCTGGCCGTACTCGAG
    9 -L--I--K--S--V--K--W--T--E--P--A--N--L--I--S--L--A--V--L--E-

   85 TTCATCAACGTTCTGGTCATCGGTGGCAACTGCCTCGTGATTGCCGCCGTCTTCTGTTCG
   29 -F--I--N--V--L--V--I--G--G--N--C--L--V--I--A--A--V--F--C--S-

                            TM II: a.a.57-79
  145 AATAAGTTGAGGAGTGTGACGAACTTCTTTATTGTCAACCTAGCTGTGGCCGATCTTCTG
   49 -N--K--L--R--S--V--T--N--F--F--I--V--N--L--A--V--A--D--L--L-

                                                      Exon 2>3R:20,700,331
  205 GTGGGTTTGGCCGTCCTACCCTTCTCAGCCACCTGGGAAGTCTTCAAGGTTTGGATATTC
   69 -V--G--L--A--V--L--P--F--S--A--T--W--E--V--F--K--V--W--I--F-

    -20,700,095        TM III: a.a.94-116
  265 GGCGATCTCTGGTGCCGCATTTGGCTGGCTGTCGATGTCTGGATGTGCACGGCATCGATC
   89 -G--D--L--W--C--R--I--W--L--A--V--D--V--W--M--C--T--A--S--I-

  325 CTGAATCTGTGTGCCATATCACTGGACCGCTATGTGGCGGTCACACGACCCGTCACCTAC
  109 -L--N--L--C--A--I--S--L--D--R--Y--V--A--V--T--R--P--V--T--Y-

                            TM IV: a.a.137-159
  385 CCAAGCATAATGTCCACGAAGAAGGCCAAGTCCTTAATCGCCGGCATTTGGGTACTCTCA
  129 -P--S--I--M--S--T--K--K--A--K--S--L--I--A--G--I--W--V--L--S-

                                                    Exon 3>3R:20,698,857-
  445 TTTTTTATTTGCTTTCCGCCGCTAGTCGGCTGGAAGGATCAAAAGGCGGTTATACAGCCG
  149 -F--F--I--C--F--P--P--L--V--G--W--K--D--Q--K--A--V--I--Q--P-

    20,698,335
  505 ACCTATCCAAAGGGAAACCATACGCTTTACTACACCACCACGATGTCAAGCTCGGAGGAT
  169 -T--Y--P--K--G--N--H--T--L--Y--Y--T--T--T--M--S--S--S--E--D-

  565 GGTCAACTAGGGTTAGATAGCATTAAGGACCAGGGCGAGGCATCCTTGCCTCCATCCCCG
  189 -G--Q--L--G--L--D--S--I--K--D--Q--G--E--A--S--L--P--P--S--P-

  625 CCCCATATCGGCAACGGCAACGCCTACAATCCCTACGATCCCGGTTTCGCACCCATCGAT
  209 -P--H--I--G--N--G--N--A--Y--N--P--Y--D--P--G--F--A--P--I--D-

  685 GGATCCGCGGAGATTCGGATTGCGGCCATTGACTCGACCAGTACTTCAACAACCGCAACC
  229 -G--S--A--E--I--R--I--A--A--I--D--S--T--S--T--S--T--T--A--T-

  745 ACCACGACGACAGCGTCCAGCTCGAGCACCACGGAAACGGAAATGGACCTCGATCTACTG
  249 -T--T--T--T--A--S--S--S--S--T--T--E--T--E--M--D--L--D--L--L-

  805 AACGCACCGCCGCAGAACAGACCCCAAACAATTTCCGGCAGTTGTCCGTGGAAGTGCGAG
  269 -N--A--P--P--Q--N--R--P--Q--T--I--S--G--S--C--P--W--K--C--E-
```

TM V: *a.a*.294-316

```
 865 CTGACCAACGATCGGGGTTATGTCCTGTACTCCGCCCTGGGCTCATTCTATATACCCATG
 289 -L--T--N--D--R--G--Y--V--L--Y--S--A--L--G--S--F--Y--I--P--M-

 925 TTCGTGATGCTCTTCTTCTACTGGCGCATCTACCGGGCTGCCGTGAGAACGACGAGAGCC
 309 -F--V--M--L--F--F--Y--W--R--I--Y--R--A--A--V--R--T--T--R--A-

                                 MI12417> Coding intron 3; 3R:20,697,059
                                          MI12417> Intracellular: a.a.338
                                 Exon 4>3R:20,693,848-20,692,947
 985 ATCAACCAGGGCTTCAAGACCACCAAGGGCAGTCCCCGCGAGTCGGGCAACAATCGAGTG
 329 -I--N--Q--G--F--K--T--T--K--G--S--P--R--E--S--G--N--N--R--V-

1045 GACGAGTCCCAGCTCATATTGCGCATTCACCGAGGAAGACCTTGCTCCACCCCCCAGCGC
 349 -D--E--S--Q--L--I--L--R--I--H--R--G--R--P--C--S--T--P--Q--R-

1105 ACGCCCCTCTCGGTGCACTCAATGTCCTCGACTCTCAGCGTGAACAGCAACGGGGGCGGG
 369 -T--P--L--S--V--H--S--M--S--S--T--L--S--V--N--S--N--G--G--G-

1165 GGTGGAGCCGTGGCCTCGGGACTGGGTGCCTCCACCGAGGATCACCTTCAGGGAGGCGCC
 389 -G--G--A--V--A--S--G--L--G--A--S--T--E--D--H--L--Q--G--G--A-

1225 CCCAAGCGGGCCACATCGATGCGCGTCTGCCGACAGCGACACGAGAAGGTGGCCATCAAG
 409 -P--K--R--A--T--S--M--R--V--C--R--Q--R--H--E--K--V--A--I--K-

1285 GTGTCCTTTCCCTCCTCCGAGAATGTCCTCGACGCAGGACAGCAGCCACAGGCATCGCCA
 429 -V--S--F--P--S--S--E--N--V--L--D--A--G--Q--Q--P--Q--A--S--P-

1345 CACTATGCGGTAATCAGTAGCGCCAACGGACGTCGTGCCTCCTTTAAGACGAGCCTCTTC
 449 -H--Y--A--V--I--S--S--A--N--G--R--R--A--S--F--K--T--S--L--F-

1405 GACATTGGCGAGACCACCTTTAATTTGGACGCAGCTGCGTCCGGTCCCGGAGACCTAGAG
 469 -D--I--G--E--T--T--F--N--L--D--A--A--A--S--G--P--G--D--L--E-

1465 ACCGGACTCTCGACCACCTCACTGTCGGCCAAGAAGCGGGCAGGCAAGCGCAGCGCCAAG
 489 -T--G--L--S--T--T--S--L--S--A--K--K--R--A--G--K--R--S--A--K-

                                                    TM VI: a.a.524-546
1525 TTTCAGGTGAAGCGGTTCCGAATGGAGACCAAGGCAGCCAAGACGCTGGCCATCATTGTG
 509 -F--Q--V--K--R--F--R--M--E--T--K--A--A--K--T--L--A--I--I--V-

1585 GGCGGCTTCATCGTTTGCTGGCTGCCCTTCTTCACGATGTATCTGATCCGGGCCTTCTGC
 529 -G--G--F--I--V--C--W--L--P--F--F--T--M--Y--L--I--R--A--F--C-

                              TM VII: a.a.556-578
1645 GACCACTGCATTCAGCCGACGGTCTTTTCGGTGCTCTTCTGGCTGGGCTACTGCAACTCG
 549 -D--H--C--I--Q--P--T--V--F--S--V--L--F--W--L--G--Y--C--N--S-

1705 GCCATTAATCCGATGATCTATGCGCTCTTCTCGAATGAGTTTCGCATCGCCTTCAAGCGG
 569 -A--I--N--P--M--I--Y--A--L--F--S--N--E--F--R--I--A--F--K--R-

1765 ATAGTGTGCAGATGCGTCTGCACCCGCAGTGGCTTCCGGGCGTCGGAGAATTTCCAGATG
 589 -I--V--C--R--C--V--C--T--R--S--G--F--R--A--S--E--N--F--Q--M-

1825 ATAGCGGCGCGTGCCCTGATGGCACCGGCAACATTCCACAAGACCATATCCGGATGCTCG
 609 -I--A--A--R--A--L--M--A--P--A--T--F--H--K--T--I--S--G--C--S-

1885 GACGACGGCGAGGGCGTGGACTTCAGCTGA
 629 -D--D--G--E--G--V--D--F--S--*-
```

Fig 1

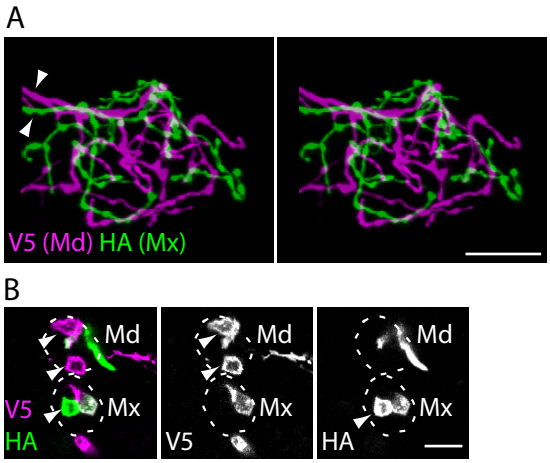

Fig 2

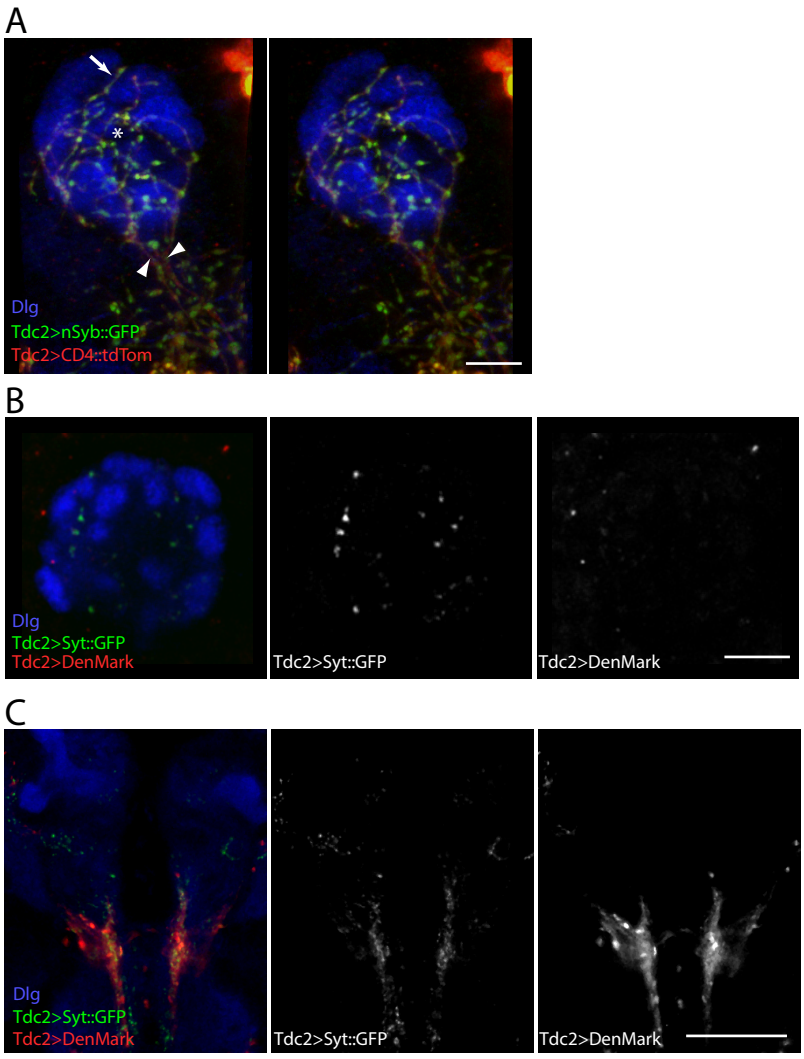

Figure 3

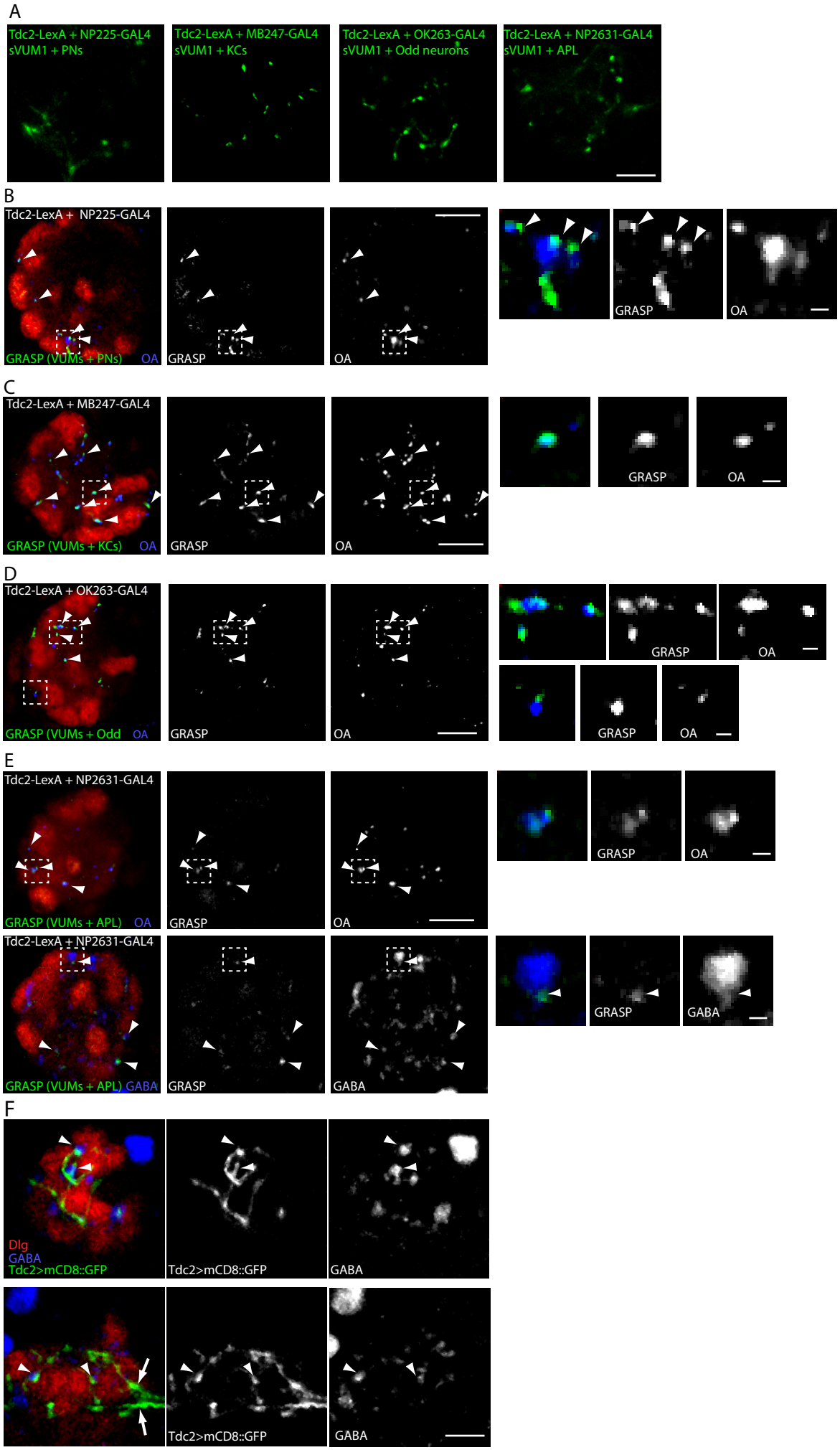

Figure 4

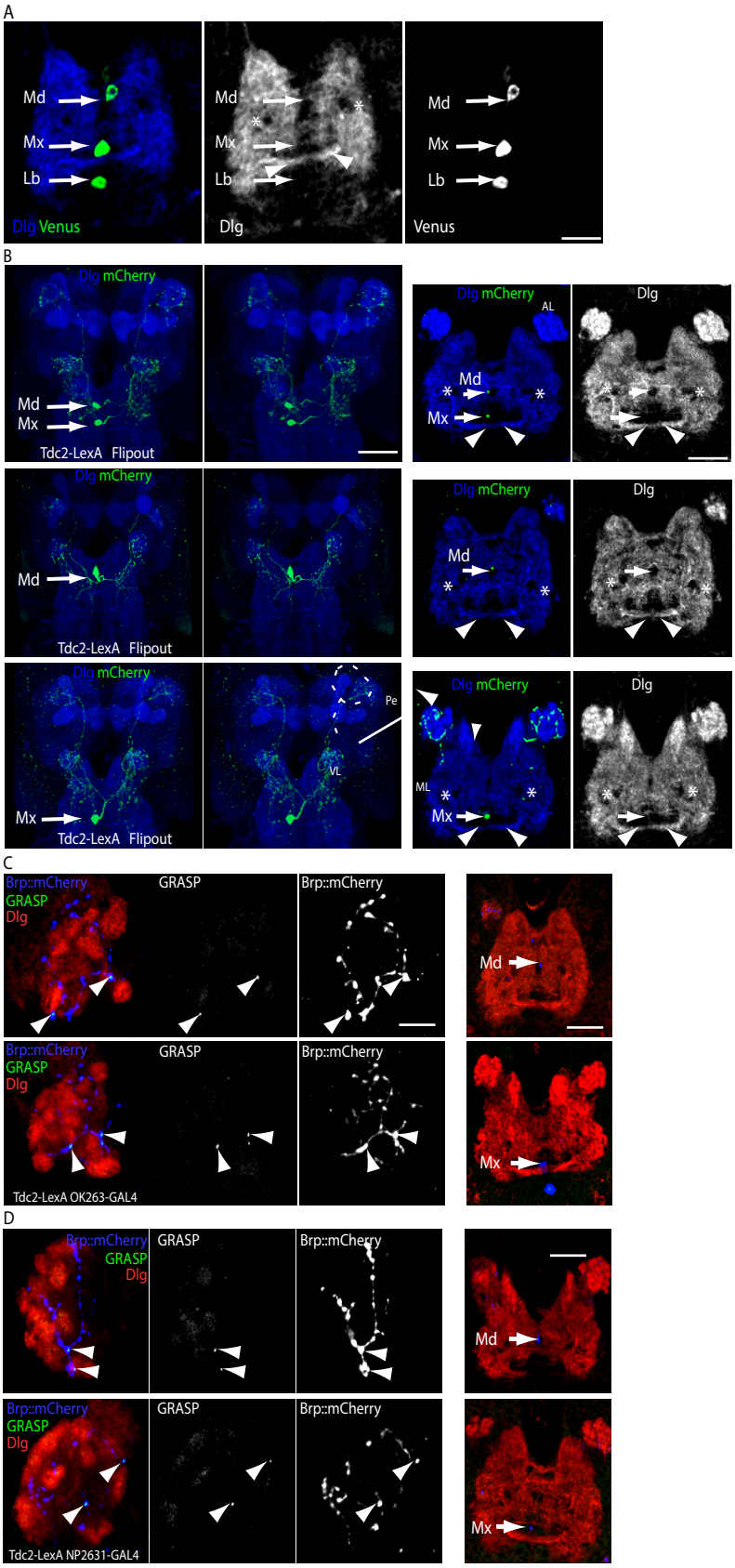

Figure 5

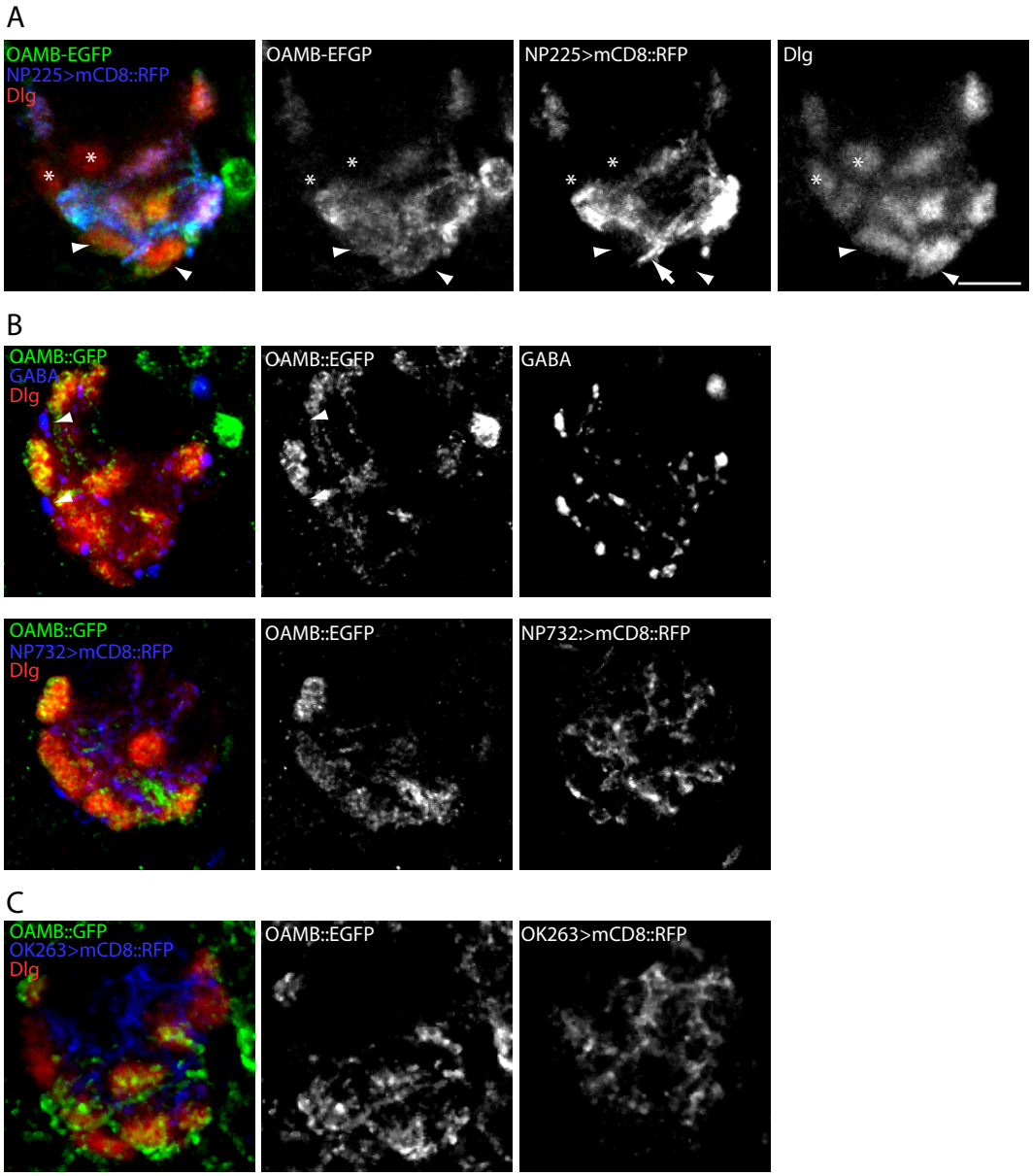

Figure 6

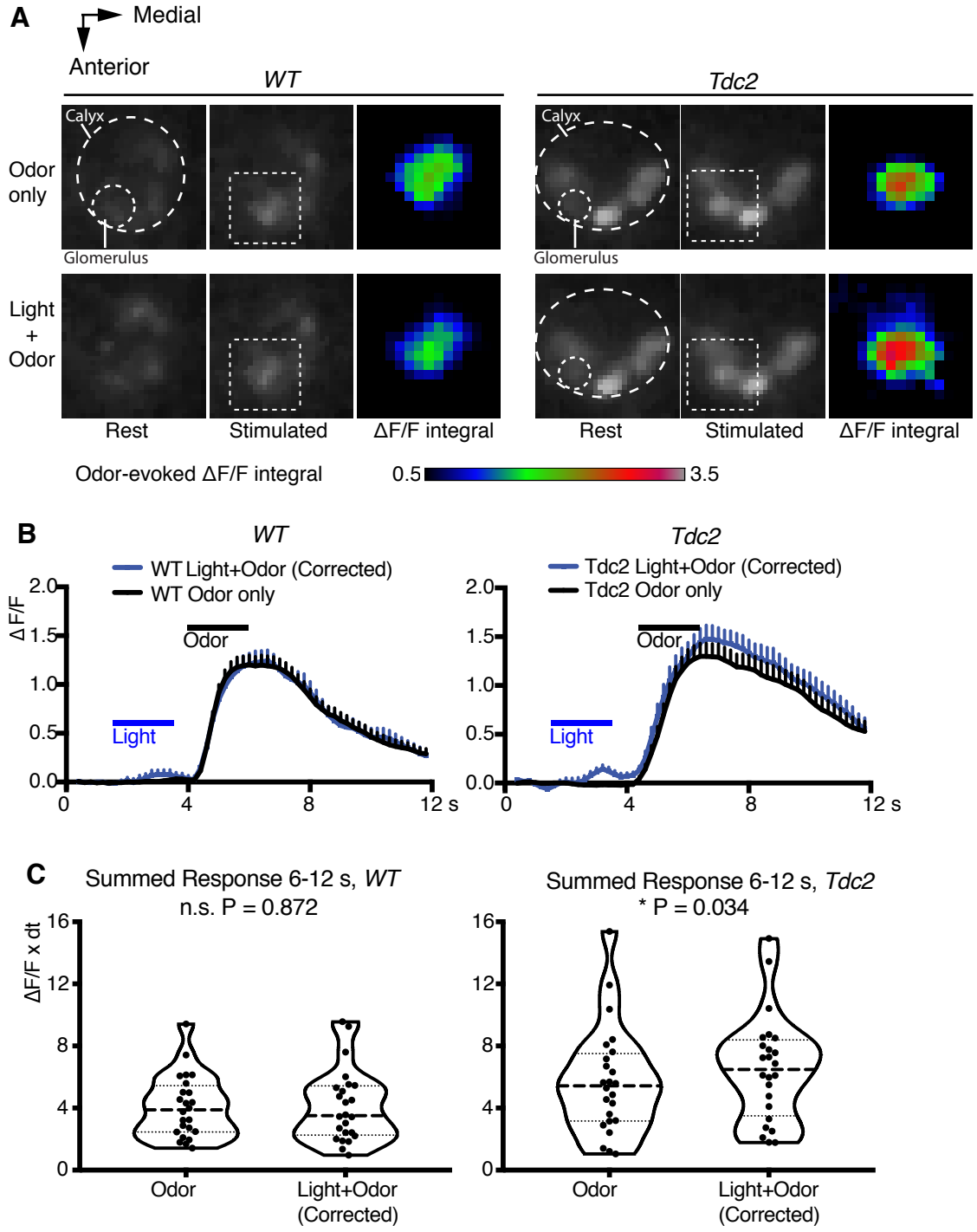

Fig ure 7

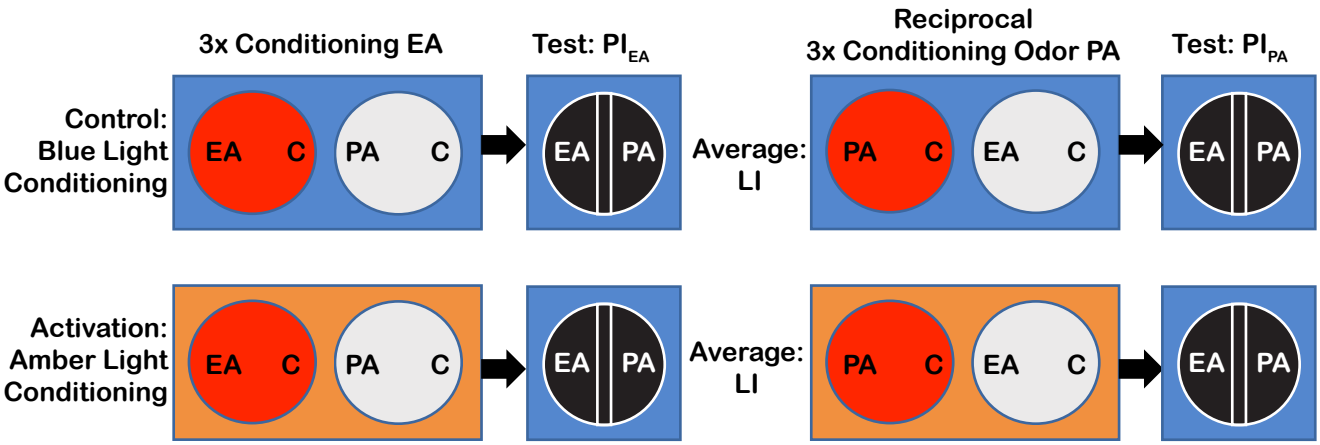

Figure 8

A

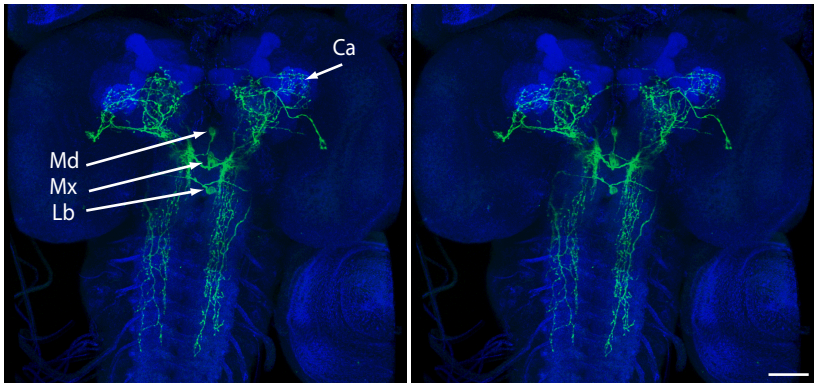

B